REPORT DOCUMENTATION PAGE

Form Approved
OMB No. 0704-0188

1. REPORT DATE *(DD-MM-YYYY)*	2. REPORT TYPE	3. DATES COVERED *(From - To)*
2/1/1997	Technical Report - Other	1/1/0001 - 1/1/0001

4. TITLE AND SUBTITLE
Second-Order Characteristic Methods for Advection-Di□fusion Equations and Comparison to Other Schemes

5a. CONTRACT NUMBER

5b. GRANT NUMBER

5c. PROGRAM ELEMENT NUMBER

6. AUTHOR(S)

5d. PROJECT NUMBER

5e. TASK NUMBER

5f. WORK UNIT NUMBER

7. PERFORMING ORGANIZATION NAME(S) AND ADDRESS(ES)
University of South Carolina Columbia SC 242

8. PERFORMING ORGANIZATION REPORT NUMBER

9. SPONSORING/MONITORING AGENCY NAME(S) AND ADDRESS(ES)
Office of Naval Research Arlington 46 242

10. SPONSOR/MONITOR'S ACRONYM(S)

11. SPONSOR/MONITOR'S REPORT NUMBER(S)

12. DISTRIBUTION/AVAILABILITY STATEMENT
1 1/1/0001 12:00:00 AM

13. SUPPLEMENTARY NOTES

14. ABSTRACT
We develop two characteristic methods for the solution of the linear advection dif
fusion equations which use a second order RungeKutta approximation of the characteristics within the framework of the EulerianLagrangian localized adjoint method□ These methods nat urally incorporate all three types of boundary conditions in their formulations□ are fully mass conservative□ and generate regularly structured systems which are symmetric and positive def inite for most combinations of the boundary conditions□ Extensive numerical experiments are

15. SUBJECT TERMS

16. SECURITY CLASSIFICATION OF:			17. LIMITATION OF ABSTRACT	18. NUMBER OF PAGES	19a. NAME OF RESPONSIBLE PERSON
a. REPORT	b. ABSTRACT	c. THIS PAGE			19b. TELEPHONE NUMBER *(Include area code)*
U	U				

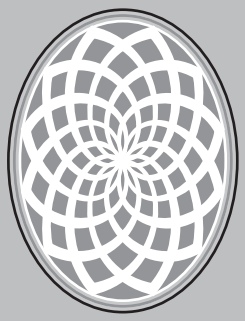

Industrial Mathematics Institute

1997:15

Second-order characteristic methods for advection-diffusion equations and comparison to other schemes

M. Al-Lawatia, R.C. Sharpley and H. Wang

IMI

Preprint Series

Department of Mathematics
University of South Carolina

Second-Order Characteristic Methods for Advection-Diffusion Equations and Comparison to Other Schemes *

Mohamed Al-Lawatia † Robert C. Sharpley ‡ Hong Wang‡

Abstract *We develop two characteristic methods for the solution of the linear advection diffusion equations which use a second order Runge-Kutta approximation of the characteristics within the framework of the Eulerian-Lagrangian localized adjoint method. These methods naturally incorporate all three types of boundary conditions in their formulations, are fully mass conservative, and generate regularly structured systems which are symmetric and positive definite for most combinations of the boundary conditions. Extensive numerical experiments are presented which compare the performance of these two Runge-Kutta methods to many other well perceived and widely used methods which include many Galerkin methods and high resolution methods from fluid dynamics.*

Key words characteristic methods, comparison of numerical methods, Eulerian-Lagrangian methods, numerical solutions of advection-diffusion equations, Runge-Kutta methods.

1 Introduction

Advection-diffusion equations are an important class of partial differential equations that arise in many scientific fields including fluid mechanics, gas dynamics, and atmospheric modeling. These equations model physical phenomenon characterized by a moving front. In fluid dynamics, for example, the movement of a solute in ground water is described by such an equation. Since these equations normally have no closed form analytical solutions, it is very important to have accurate numerical approximations. When diffusion dominates the physical process, standard finite difference methods (FDM) and finite element methods (FEM) work well in solving these equations. However, when advection is the dominant process, these equations present many numerical difficulties. In fact, standard finite element and finite difference methods produce solutions which exhibit non-physical oscillations, excessive numerical diffusion which smears out sharp fronts, or a combination of both [21, 35].

Many specialized schemes have been developed to overcome the difficulties mentioned. One class of these methods, usually referred to as the class of *Eulerian methods*, uses an Eulerian fixed grid and improved techniques, such as *upstream weighting*, to generate more

*This research was supported in part by DOE Grant No. DE-FG05-95ER25266, by ONR Grant No. N00014-94-1-1163, and by the funding from the Mobil Technology Company.

†Department of Mathematics and Statistics, Sultan Qaboos University, P.O. Box 36, Al-Khod Postal Code 123, Muscat, Sultanate of Oman

‡Department of Mathematics, University of South Carolina, Columbia, South Carolina 29208, U.S.A.

accurate approximations. Most of the methods in this class are characterized by ease of formulation and implementation, however their solutions suffer from excessive time truncation errors. Moreover, they put a strong limitation on the Courant number and hence require very small time steps to generate stable solutions. Among these methods are the Petrov-Galerkin FEM methods [1, 4, 9, 55] which are improvements over the standard Galerkin FEM that incorporate *upwinding* in the space of the test functions. Also included in the class of Eulerian methods are the streamline diffusion FEM methods (SDM) [5, 19, 26, 31, 32, 33, 35, 36] and the continuous and discontinuous Galerkin methods (CGM, DGM) [23, 34, 37, 42, 43]. The SDM improve over the standard space-time Galerkin FEM by adding a multiple of the (linearized) hyperbolic operator of the problem considered to the standard test functions. Thus they add numerical diffusion only in the direction of the streamlines. The SDM formulations have a free parameter which determines the amount of diffusion applied and therefore has a great effect on the accuracy of these methods. In practice, this parameter should be large enough to avoid oscillations in the solution, but not too large to damp the solution. A clear choice of this parameter is not known, in general, and is heavily problem dependent. The CGM and DGM are well suited for purely hyperbolic equations and recently have been extended to solve the advection-diffusion equations. They are space-time explicit methods in which, starting with the initial time solution and Dirichlet data at the inflow boundary, one would successively iterate over the elements of a quasi-uniform triangulation of the space-time domain in an order consistent with the domain, solving a local system over each element. In addition to the methods mentioned above, the class of Eulerian methods includes the high resolution methods in fluid dynamics such as the Godunov methods, the total variation diminishing methods (TVD), and the essentially non-oscillatory methods (ENO) [10, 11, 12, 18, 24, 27, 46, 47, 48, 49]. These methods, as well as the CGM and DGM, are well suited for advection-diffusion equations with small diffusion coefficients and in general impose an extra stability restriction on the size of the time step taken based on the magnitude of this coefficient. Therefore, they are very sensitive to changes in the diffusion coefficient, which in practical problems is likely to have large values at certain points.

Another class of methods, usually known as *characteristic methods*, makes use of the hyperbolic nature of the governing equation. These methods use a combination of Eulerian fixed grids to treat the diffusive component, and Lagrangian coordinates by tracking particles along the characteristics to treat the advective component. Included in this class are the Eulerian-Lagrangian methods (ELM), the modified methods of characteristics (MMOC), and the operator splitting methods [2, 13, 17, 20, 21, 25, 30, 38, 39, 40, 41, 50, 56]. These methods have the desirable advantage of alleviating the restrictions on the Courant number, thus allowing for large time steps. Furthermore, the Lagrangian treatment in these methods greatly reduces the time truncation errors which are present in Eulerian methods. On the other hand these methods have difficulty in conserving mass and treating general boundary conditions. The Eulerian-Lagrangian localized adjoint methods (ELLAM) were developed as an improved extension of the characteristic methods that maintains their advantages but enhances their performance by conserving mass and treating general boundary conditions naturally in their formulations. The first ELLAM formulations were developed for constant coefficient advection-diffusion equations [7, 44]. The strong potential that these FEM based formulations and their numerical results have demonstrated have led to the development of additional formulations for variable-coefficient advection diffusion equations [45, 51] and for nonlinear equations [14] as well as finite volume formulations [8, 28]. However, because

the characteristics for variable-coefficient advection-diffusion equations cannot be tracked exactly in general, many characteristic and ELLAM methods that have been developed use a backward Euler approximation for these characteristics due to its simplicity and stability. These (backward Euler) schemes are second order accurate in space but only first order accurate in time.

An ELLAM based formulation which uses a second order approximation for the characteristics was developed recently for first-order advection-reaction equations [54]. This formulation was shown to be of second order in both space and time. Unlike the first-order equations, similar treatment for the advection-diffusion equations is more problematic since one needs to treat the diffusive component and its partial derivatives (with respect to the rectangular and characteristic coordinates) carefully along the characteristics to produce systems having desirable structure. In addition, boundary treatment is more involved because at both the inflow and outflow boundary data can be specified in many forms which then need to be incorporated into the formulations. In this paper we develop characteristic methods for the one-dimensional linear advection-diffusion equations, based on a second order Runge-Kutta approximation of the characteristics. We present a backward tracking (BRKC) and a forward tracking (FRKC) Runge-Kutta characteristic scheme, both of which are mass conservative and incorporate boundary conditions naturally in their formulations. These methods, which can be thought of as generalizations of the ELLAM schemes, generate tridiagonal (regularly structured in multi-dimensions) matrices which are symmetric (except at the inflow boundary) and positive definite that can be solved efficiently. Moreover, we provide the results of some extensive numerical experiments which compare the performance of the two methods developed to many of the methods mentioned above.

This paper is organized as follows. In Section 2 we develop a reference equation based on exact characteristic tracking. In Section 3 we present the two characteristic schemes BRKC and FRKC which are based on a backward tracking and a forward tracking algorithm, respectively. We also give a detailed description of boundary treatment, in addition to some numerical experiments which demonstrate the order of convergence of the two schemes. In Section 4 we give a brief description of some well studied and widely used methods which are known to give good approximations to the advection diffusion equations. Section 5 contains the results of the numerical experiments that compare the performance of the two schemes developed in Section 3 and the other methods described in Section 4.

2 Development of the Method

We consider the one-dimensional linear variable-coefficient advection-diffusion equation

$$\begin{aligned} \mathcal{L}u \equiv u_t + (V(x,t)u - D(x,t)u_x)_x &= f(x,t), \quad x \in (a,b), \;\; t \in [0,T], \\ u(x,0) &= u_o(x), \qquad x \in [a,b], \end{aligned} \tag{2.1}$$

where $V(x,t)$ and $D(x,t)$ are the velocity field and the diffusion coefficient, respectively. $D(x,t)$ is assumed to be positive throughout the domain. To simplify our presentation, we also assume $V(a,t)$ and $V(b,t)$ are positive, i.e. we set $x = a$ and $x = b$ to be the inflow and outflow boundaries, respectively. In many advection-dominated applications,

$|D(x,t)| << |V(x,t)|$, therefore, methods devised to solve equation (2.1) should handle this case accurately. We consider general boundary conditions with any combination of Dirichlet, Neumann, or Robin conditions at the inflow and outflow boundaries. The function $g(t)$ is used to denote the time dependence to specify the boundary condition at $x = a$ and $h(t)$ for the outflow boundary at $x = b$. The Dirichlet, Neumann, and Robin conditions are formulated by the requirements

$$\begin{aligned} u(c,t) &= \phi_1(t), \quad t \in (0,T], \\ -(Du_x)(c,t) &= \phi_2(t), \quad t \in (0,T], \\ (Vu - Du_x)(c,t) &= \phi_3(t), \quad t \in (0,T], \end{aligned} \tag{2.2}$$

respectively, where $\phi = g$ when $c = a$ and $\phi = h$ when $c = b$.

2.1 Variational Formulation and Characteristic Curves

The domain of problem (2.1), is $[a,b] \times [0,T]$ which we partition in space and time as follows:

$$\begin{array}{ccccccccc} 0 & = & t^0 & < & t^1 & < \ldots < & t^N & = & T, \\ a & = & x_0^n & < & x_1^n & < \ldots < & x_{I_n}^n & = & b, \quad n = 0,1,\ldots,N\ , \end{array} \tag{2.3}$$

for positive integers N, I_n $(n = 0, 1, ..., N)$. We utilize space-time test functions that vanish outside $[a,b] \times (t^n, t^{n+1}]$, which enables us to concentrate on one time period $(t^n, t^{n+1}]$. Our test functions are discontinuous in time and allow for different meshes at different time periods. For notational simplicity, we suppress the temporal index on the grid. The variational formulation of equation (2.1) on the domain $\Omega = [a,b] \times (t^n, t^{n+1}]$, obtained by multiplying that equation by a test function w (which we describe in more detail below) and integrating by parts, becomes

$$\begin{aligned} &\int_a^b u(x,t^{n+1})w(x,t^{n+1})\,dx + \int_{t^n}^{t^{n+1}} \int_a^b Du_x w_x\,dxdt \\ &\qquad + \int_{t^n}^{t^{n+1}} (Vu - Du_x)w\,|_a^b\,dt - \int_{t^n}^{t^{n+1}} \int_a^b u(w_t + Vw_x)\,dxdt \\ &= \int_a^b u(x,t^n)w(x,t_+^n)\,dx + \int_{t^n}^{t^{n+1}} \int_a^b fw\,dxdt, \end{aligned} \tag{2.4}$$

where we use the notation $w(x,t_+^n) = \lim_{t \to t_+^n} w(x,t)$ due to the discontinuity of $w(x,t)$ at time t^n.

The principle of the localized adjoint methods (LAM) requires the test functions to be chosen from the solution space of the homogeneous adjoint equation

$$\mathcal{L}^* w \equiv -w_t - V(x,t)w_x + (D(x,t)w_x)_x = 0. \tag{2.5}$$

However, the solution space of this equation is infinite dimensional. Thus we need to split this equation to determine a finite number of test functions. In fact, different splittings lead

to different approximation schemes (see [7, 52]). Due to the Lagrangian nature of the exact solution, a natural splitting is

$$\begin{aligned} w_t + V(x,t)w_x &= 0, \\ (D(x,t)w_x)_x &= 0. \end{aligned} \tag{2.6}$$

The ELLAM generalizes the framework of the localized adjoint methods by requiring the test functions to satisfy the first equation in (2.6) exactly or even approximately (so that the last term on the left hand side of equation (2.4) vanishes exactly or approximately). However, the ELLAM does not require the second equation in (2.6) to be satisfied, thus one does not have to choose the test functions $w(x,t)$ to be of a complicated form in space. In our formulation, we choose the test functions to be piecewise linear in space, as in the linear standard FEM, and to be constant along characteristics which we discuss below.

The characteristic curves of (2.1) are given by the solutions of initial value problems for the ordinary differential equation

$$\frac{dy}{dt} = V(y,t). \tag{2.7}$$

We denote the characteristic curve emanating from a given point $(\bar{x},\bar{t})$ with $t \in [t^n, t^{n+1}]$, by

$$y = X(\theta;\bar{x},\bar{t}), \tag{2.8}$$

where θ is the time position parameter along that characteristic. Furthermore, we introduce below some notation that is described by the following relations

$$\begin{aligned} \tilde{x} &= X(t^{n+1};x,t^n), \\ x^* &= X(t^n;x,t^{n+1}), \\ b^*(t) &= X(t^n;b,t), \\ a &= X(t^*(x);x,t^{n+1}), \\ b &= X(\tilde{t}(x);x,t^n). \end{aligned} \tag{2.9}$$

We define $\tilde{x}$ and x^* as the head (using forward tracking) and the foot (using backward tracking), respectively, of the characteristics. The foot of a characteristic with head on the outflow boundary is denoted by $b^*(t)$ for $t \in [t^n, t^{n+1}]$. We also define $\tilde{t}(x)$ and $t^*(x)$ as the exit times of the characteristics $X(\theta;x,t^n)$ and $X(\theta;x,t^{n+1})$ at the outflow and inflow boundaries, respectively (see Figure 1.b). The general time increment over the domain may then be written as

$$\Delta t(x) := \tilde{t}(x) - t^*(x),$$

where we define $t^*(x) = t^n$ for characteristics with feet not on the inflow boundary, and similarly $\tilde{t}(x) = t^{n+1}$ for characteristics with heads not belonging to the outflow boundary. By implicitly differentiating the fourth relation in (2.9) for $t^*(x)$ with respect to x, and the relation $X(\theta;b,t) = b + \int_t^\theta V(X(s;b,t),s)ds$, for characteristics $X(\theta;b,t)$ with $\theta \in [t^n, t]$ originating at points (b,t) on the outflow boundary, with respect to t, we get the following

equations (for partial derivatives of the characteristics)

$$\begin{aligned} X_x(t^*(x); x, t^{n+1}) &= -V(a, t^*(x))\frac{dt^*(x)}{dx}, \\ X_t(\theta; b, t)|_{\theta=t} &= -V(b, t), \end{aligned} \tag{2.10}$$

in respective order. In the following section, we consider approximations of the characteristics, defined by second order Runge-Kutta approximations.

2.2 Reference Equation

After we have introduced the notion of the characteristics, we are able to find a reference equation by expanding certain of the integrals in the variational formulation (2.4). First we assume that we can exactly track the characteristics, thus the same reference equation is generated if we use either forward or backward tracking algorithms.

2.2.1 Treatment of the Source Term

We start with the source term (second term on the right hand side of equation (2.4)) which we break as follows,

$$\int_{t^n}^{t^{n+1}} \int_a^b fw \, dxdt = \iint_{\Omega_1} fw \, dyds + \iint_{\Omega_2} fw \, dyds + \iint_{\Omega_3} fw \, dyds. \tag{2.11}$$

Here the region Ω_1 represents all points which lie on characteristics with feet on the inflow boundary, Ω_3 represents all points on characteristics with heads on the outflow boundary, and finally Ω_2 represents the remainder of Ω (see Figure 1.a). For clarity of presentation, we use the variable y to represent the spatial coordinate of any point in Ω, and reserve x for points on the spatial mesh of Ω at time t^n or t^{n+1}, representing either heads or feet of characteristics. Similarly we let s denote the temporal variable instead of t, which we reserve for the temporal coordinate of heads or feet of characteristics which lie on either the inflow or outflow boundary. The general time increment can also be described for points x at time t^{n+1} or time t^n in respective order by $\Delta t^{(I)}(x)$ and $\Delta t^{(O)}(x)$ which are defined as follows

$$\begin{aligned} \Delta t^{(I)}(x) &= t^{n+1} - t^*(x), \qquad x \in [a, b], \\ \Delta t^{(O)}(x) &= \tilde{t}(x) - t^n, \qquad x \in [a, b], \end{aligned} \tag{2.12}$$

where $t^*(x)$ and $\tilde{t}(x)$ extend to t^n and t^{n+1}, respectively, if the characteristics that define them lie in Ω_2. With the change of variable $y = y(x, s) = X(s; x, t^{n+1})$ for the first integral

on the right hand side of (2.11), we obtain

$$\begin{aligned}
&\iint_{\Omega_1} f(y,s)\, w(y,s)\, dyds \\
&\quad = \int_a^{\tilde{a}} \int_{t^*(x)}^{t^{n+1}} f(X(s;x,t^{n+1}),s)\, w(X(s;x,t^{n+1}),s)\, X_x(s;x,t^{n+1})\, dsdx \\
&\quad = \int_a^{\tilde{a}} \frac{\Delta t^{(I)}(x)}{2} \Big(f(x,t^{n+1})\, w(x,t^{n+1}) + \\
&\qquad\qquad f(a,t^*(x))\, w(a,t^*(x))\, X_x(t^*(x);x,t^{n+1}) \Big)\, dx + E_{f,\Omega_1}(w) \\
&\quad = \int_a^{\tilde{a}} \frac{\Delta t^{(I)}(x)}{2} f(x,t^{n+1})\, w(x,t^{n+1})\, dx \\
&\qquad + \int_{t^n}^{t^{n+1}} \frac{(t^{n+1}-t)}{2} f(a,t)\, w(a,t)\, V(a,t)\, dt + E_{f,\Omega_1}(w),
\end{aligned} \tag{2.13}$$

where in the second equality we used a trapezoidal approximation for the inner integral whose error $E_{f,\Omega_1}(w)$ is given below. In the last equality we moved the second integral to the inflow boundary by the change of variable $a = X(t^*(x);x,t^{n+1})$ and the first equation in (2.10). The trapezoidal error term introduced is given by

$$\begin{aligned}
&E_{f,\Omega_1}(w) = \\
&\quad \int_a^{\tilde{a}} \int_{t^*(x)}^{t^{n+1}} \frac{(t^*(x)-s)(t^{n+1}-s)}{2} \frac{d^2}{ds^2} \Big[X_x(s;x,t^{n+1}) f(X(s;x,t^{n+1}),s) \Big]\, w(x,t^{n+1})\, dsdx,
\end{aligned} \tag{2.14}$$

since w is constant along characteristics. With the same change of variable, $y = X(s;x,t^{n+1})$, and similar treatment as in (2.13), we expand the second integral on the right hand side of equation (2.11) to get

$$\begin{aligned}
&\iint_{\Omega_2} f(y,s)\, w(y,s)\, dyds \\
&\quad = \int_{\tilde{a}}^{b} \int_{t^n}^{t^{n+1}} f(X(s;x,t^{n+1}),s)\, w(X(s;x,t^{n+1}),s)\, X_x(s;x,t^{n+1})\, dsdx \\
&\quad = \int_{\tilde{a}}^{b} \frac{\Delta t}{2} \left(f(x,t^{n+1})\, w(x,t^{n+1}) + f(x^*,t^n)\, w(x^*,t_+^n)\, \frac{dx^*}{dx} \right)\, dx + E_{f,\Omega_2}(w) \\
&\quad = \int_{\tilde{a}}^{b} \frac{\Delta t}{2} f(x,t^{n+1})\, w(x,t^{n+1})\, dx + \int_a^{b^*} \frac{\Delta t}{2} f(x,t^n)\, w(x,t_+^n)\, dx + E_{f,\Omega_2}(w),
\end{aligned} \tag{2.15}$$

where we have used the fact that $\frac{dx^*}{dx} = X_x(t^n;x,t^{n+1})$. In this expression the trapezoidal error term is given by

$$\begin{aligned}
&E_{f,\Omega_2}(w) = \\
&\quad \int_{\tilde{a}}^{b} \int_{t^n}^{t^{n+1}} \frac{(t^n-s)(t^{n+1}-s)}{2} \frac{d^2}{ds^2} \Big[X_x(s;x,t^{n+1}) f(X(s;x,t^{n+1}),s) \Big]\, w(x,t^{n+1})\, dsdx.
\end{aligned} \tag{2.16}$$

The treatment of the source term over Ω_3 is slightly different since for the characteristics, we backtrack from points originating on the outflow boundary. With the change of variable

$y = X(s;b,t)$, the third term on the right hand side of (2.11) becomes

$$\begin{aligned}
&\iint_{\Omega_3} f(y,s)\, w(y,s)\, dyds \\
&\quad = \; -\int_{t^n}^{t^{n+1}} \int_{t^n}^{t} f(X(s;b,t),s)\, w(X(s;b,t),s)\, X_t(s;b,t)\, dsdt \\
&\quad = \; -\int_{t^n}^{t^{n+1}} \frac{(t-t^n)}{2} \Big(f(b,t)\, w(b,t)\, X_t(t;b,t) \\
&\qquad\qquad + \; f(X(t^n;b,t),t^n)\, w(X(t^n;b,t),t_+^n)\, X_t(t^n;b,t) \Big)\, dt + \; E_{f,\Omega_3}(w) \\
&\quad = \; \int_{t^n}^{t^{n+1}} \frac{(t-t^n)}{2} V(b,t)\, f(b,t)\, w(b,t)\, dt \\
&\qquad + \int_{b^*}^{b} \frac{\Delta t^{(O)}(x)}{2} f(x,t^n)\, w(x,t_+^n)\, dx + E_{f,\Omega_3}(w),
\end{aligned} \tag{2.17}$$

where in the last equality we used the second equation in (2.10) for the first integral and the change of variable $x = X(t^n;b,t)$ for the second. The trapezoidal error term introduced is given by

$$E_{f,\Omega_3}(w) = \int_{t^{n+1}}^{t^n} \int_{t^n}^{t} \frac{(t^n-s)(t-s)}{2} \frac{d^2}{ds^2} \left[X_t(s;b,t)\, f(X(s;b,t),s) \right] w(b,t)\, dsdt. \tag{2.18}$$

2.2.2 Treatment of the Diffusion Term

Next we treat the second term on the left hand side of equation (2.4), which we break, similar to the source term in (2.11), over the three subdomains Ω_i $(i = 1,2,3)$ discussed above. Due to the similarity in the treatment of this integral over Ω_1 and Ω_2, we combine the two and use the same change of variable $y = X(s;x,t^{n+1})$ as before, and obtain

$$\begin{aligned}
&\iint_{\Omega_1 \cup \Omega_2} D(y,s)\, u_y(y,s)\, w_y(y,s)\, dyds \\
&\quad = \; \int_a^b \int_{t^*(x)}^{t^{n+1}} X_x(s;x,t^{n+1})\, (Du_X)(X(s;x,t^{n+1}),s)\, w_X(X(s;x,t^{n+1}),s)\, dsdx \\
&\quad = \; \int_{\tilde{a}}^b \frac{\Delta t}{2} \Big((Du_x)(x,t^{n+1})\, w_x(x,t^{n+1}) + X_x(t^*(x);x,t^{n+1}) \times \\
&\qquad (Du_X)(X(t^*(x);x,t^{n+1}),t^*(x))\, w_X(X(t^*(x);x,t^{n+1}),t^*(x)) \Big)\, dx \\
&\qquad + \int_a^{\tilde{a}} \Delta t^{(I)}(x)\, (Du_x)(x,t^{n+1})\, w_x(x,t^{n+1})\, dx + E_{D,\Omega_{1,2}}(w) \\
&\quad = \; \int_a^{\tilde{a}} \Delta t^{(I)}(x)\, (Du_x)(x,t^{n+1})\, w_x(x,t^{n+1})\, dx + \int_{\tilde{a}}^b \frac{\Delta t}{2} (Du_x)(x,t^{n+1})\, w_x(x,t^{n+1})\, dx \\
&\qquad + \int_a^{b^*} \frac{\Delta t}{2} (Du_x)(x,t^n)\, w_x(x,t_+^n)\, dx + E_{D,\Omega_{1,2}}(w),
\end{aligned} \tag{2.19}$$

where in the second equality we used a backward Euler approximation for the integral over $(a,\tilde{a})$ and a trapezoidal approximation over $(\tilde{a},b)$ with error given below, and in the third

equality we made the change $w_x(X(s;x,t^{n+1}),s) = w_X(X(s;x,t^{n+1}),s)\times\ X_x(s;x,t^{n+1})$. The error term in (2.19) is given by

$$
\begin{aligned}
&E_{D,\Omega_{1,2}}(w) = \\
&\quad -\int_a^{\tilde{a}} \left[\int_{t^*(x)}^{t^{n+1}} \int_s^{t^{n+1}} \frac{d}{d\theta}(Du_x)(X(\theta;x,t^{n+1}),\theta) d\theta ds \right] w_x(x,t^{n+1})\, dx \\
&\quad +\int_{\tilde{a}}^{b}\int_{t^n}^{t^{n+1}} \frac{(t^n-s)(t^{n+1}-s)}{2}\frac{d^2}{ds^2}\left[(Du_x)(X(s;x,t^{n+1}),s)\right] w_x(x,t^{n+1})\, dsdx.
\end{aligned}
\tag{2.20}
$$

Using a trapezoidal approximation for this diffusive flux term over $(a,\tilde{a})$ when the inflow boundary condition is Dirichlet or Robin condition introduces unknowns on the inflow boundary and severely complicates the scheme. Therefore we chose to use only backward Euler approximation on that interval. Neumann inflow condition on the other hand allows us to use the more accurate trapezoidal approximation for the diffusive integral uniformly over the whole spatial domain. This treatment does not lead to any non-symmetric terms in the formulation. Details of this treatment and boundary implementation are discussed in the following section.

Finally we treat remaining diffusion integral over Ω_3. With the change of variable $y = X(s;b,t)$ this integral becomes

$$
\begin{aligned}
&\iint_{\Omega_3} D(y,s)\, u_y(y,s)\, w_y(y,s)\, dyds \\
&\quad = \quad -\int_{t^n}^{t^{n+1}} \int_{t^n}^{t} X_t(s;b,t)\, (Du_X)(X(s;b,t),s)\, w_X(X(s;b,t),s)\, dsdt \\
&\quad = \quad -\int_{t^n}^{t^{n+1}} \frac{(t-t^n)}{2}\Big((Du_x)(b,t)\, w_t(b,t) \\
&\qquad\qquad +X_t(t^n;b,t)\, (Du_X)(X(t^n;b,t),t^n)\, w_X(X(t^n;b,t),t^n_+)\Big)\, dt + E_{D,\Omega_3}(w) \\
&\quad = \quad -\int_{t^n}^{t^{n+1}} \frac{(t-t^n)}{2}(Du_x)(b,t)\, w_t(b,t)\, dt \\
&\qquad\quad +\int_{b^*}^{b} \frac{\Delta t^{(O)}(x)}{2}(Du_x)(x,t^n)\, w_x(x,t^n_+)\, dx \quad + \ E_{D,\Omega_3}(w),
\end{aligned}
\tag{2.21}
$$

where in the second equality, we have used the relation $w_X(b,t)X_t(t;b,t) = w_t(b,t)$ for the first integral. The error term E_{D,Ω_3} is given by,

$$
\begin{aligned}
&E_{D,\Omega_3}(w) = \\
&\qquad \int_{t^n}^{t^{n+1}} \int_{t^n}^{t} \frac{(s-t^n)(t-s)}{2}\frac{d^2}{ds^2}\left[(Du_x)(X(s;b,t),s) w_t(X(s;b,t),s)\right]\, dsdt.
\end{aligned}
\tag{2.22}
$$

2.2.3 Assembly of the Reference Equation

Substituting the integrals expanded in equations (2.13), (2.15), (2.17), (2.19) and (2.21) back into the variational equation (2.4) yields the following reference equation

$$\begin{aligned}
&\int_a^b u(x,t^{n+1})\, w(x,t^{n+1})\, dx + \int_a^{\tilde{a}} \Delta t^{(I)}(x)\, (Du_x)(x,t^{n+1})\, w_x(x,t^{n+1})\, dx \\
&\quad + \int_{\tilde{a}}^b \frac{\Delta t}{2}\, (Du_x)(x,t^{n+1})\, w_x(x,t^{n+1})\, dx \\
&\quad + \int_a^b \frac{\Delta t^{(O)}(x)}{2}\, (Du_x)(x,t^n)\, w_x(x,t_+^n)\, dx - \int_{t^n}^{t^{n+1}} \frac{(t-t^n)}{2} (Du_x)(b,t)\, w_t(b,t)\, dt \\
&\quad + \int_{t^n}^{t^{n+1}} (Vu - Du_x)(b,t)\, w(b,t)\, dt - \int_{t^n}^{t^{n+1}} (Vu - Du_x)(a,t)\, w(a,t)\, dt \\
= \;& \int_a^b u(x,t^n)\, w(x,t_+^n)\, dx + \int_a^b \frac{\Delta t^{(I)}(x)}{2} f(x,t^{n+1})\, w(x,t^{n+1})\, dx \\
&\quad + \int_a^b \frac{\Delta t^{(O)}(x)}{2} f(x,t^n)\, w(x,t_+^n)\, dx + \int_{t^n}^{t^{n+1}} \frac{(t^{n+1}-t)}{2} V(a,t)\, f(a,t)\, w(a,t)\, dt \\
&\quad + \int_{t^n}^{t^{n+1}} \frac{(t-t^n)}{2} V(b,t)\, f(b,t)\, w(b,t)\, dt \;\; - \;\; E(w) + \; R_o(w).
\end{aligned} \tag{2.23}$$

The last two terms in equation (2.23) are $E(w) = \sum_{i=1}^3 (E_{f,\Omega_i} + E_{D,\Omega_i})$ which represents the collective approximation error and $R_o(w) = \int_{t^n}^{t^{n+1}} \int_a^b u\,(w_t + V w_x)\; dxdt$ represents the adjoint term which in our case vanishes by equation (2.6).

3 Numerical Approximation

Since we do not impose a particular form for the velocity field $V(x,t)$, explicitly solving the ordinary differential equation (2.7) which defines the characteristics is not possible in general and introduces additional difficulty. Therefore in our numerical approximation of the solution of the advection diffusion equation (2.1), we consider an approximation of the characteristics $X(\theta;\bar{x},\bar{t})$ which is based on a second order Runge-Kutta approximation known as Heun's method. In particular, we define the approximate characteristic curve emanating from a point $(\bar{x},\bar{t})$, with $\bar{t} \in [t^n, t^{n+1}]$, by

$$Y(\theta;\bar{x},\bar{t}) = \bar{x} - \frac{(\bar{t}-\theta)}{2}\left[V(\bar{x},\bar{t}) + V(\bar{x} - (\bar{t}-\theta)V(\bar{x},\bar{t}),\theta)\right]. \tag{3.1}$$

Furthermore, if the Courant number $Cr = \max(V)\Delta t/\Delta x$ is at least 2, we partition the outflow boundary $\{x = b,\ t \in [t^n, t^{n+1}]\}$ as follows:

$$t_i = \begin{cases} t^{n+1} - (i-I)\Delta x/\max(V), & i = I, \ldots, I + IC - 1, \\ t^n, & i = I + IC, \end{cases} \tag{3.2}$$

where IC in this case is the integer part of Cr. When no subdivision of the outflow boundary is introduced ($Cr < 2$), we let $IC = 1$ so that both cases are treated uniformly. This partition introduces some unknowns on the outflow boundary, however it has the advantage of insuring

that the schemes we develop are suitable even for large Courant numbers. We define the test functions at time t^{n+1} as hat functions given by

$$w_i(x,t^{n+1}) = \begin{cases} \dfrac{x-x_{i-1}}{\Delta x_i}, & x \in [x_{i-1},x_i], \\ \dfrac{x_{i+1}-x}{\Delta x_{i+1}}, & x \in [x_i,x_{i+1}], \\ 0, & \text{otherwise}, \end{cases} \tag{3.3}$$

for $i = 0,\ldots,I-1$. At the outflow boundary the test functions are given by,

$$w_i(b,t) = \begin{cases} \dfrac{t_{i-1}-t}{\Delta t_i}, & t \in [t_{i-1},t_i], \\ \dfrac{t-t_{i+1}}{\Delta t_{i+1}}, & t \in [t_i,t_{i+1}], \\ 0, & \text{otherwise}, \end{cases} \tag{3.4}$$

for $i = I+1,\ldots,I+IC$. Here $\Delta x_i = x_i - x_{i-1}$ and $\Delta t_i = t_{i-1} - t_i$. For the interior of the domain Ω, we extend these test functions defined by (3.3) and (3.4) to be constant along the approximate characteristics. The test function w_I is a combination of both, that is, $w_I(x,t^{n+1})$ is defined by (3.3) for the interval $[x_{I-1},x_I]$, and $w_I(b,t)$ is defined by (3.4) on the interval $[t_{I+1},t^{n+1}]$.

The numerical schemes are based on approximating the exact solution u, which satisfies the reference equation (2.23), by a piecewise linear function U which satisfies a similar equation with two differences: (i) the new equation will be developed using the change of variables resulting from the approximate characteristic tracking given by (3.1), and (ii) the error and adjoint terms, similar to $E(w)$ and R_o in (2.23), are not included. Since the terms neglected contribute global errors which are of order $O((\Delta x)^2 + (\Delta t)^2)$, the resulting schemes will be of desired accuracy. In the following two subsections we develop two schemes to solve the advection-diffusion equation (2.1) based on backward and forward characteristic tracking, respectively. Here we emphasize that the test functions defined above are constant along the approximate characteristics.

3.1 Backtracking Runge-Kutta characteristic scheme

The first numerical scheme (BRKC) is based on a backward tracking of characteristics. We first let the domains Ω_i be defined in a similar manner as before, but use the approximate characteristics $Y(\theta;x,t^{n+1})$ in place of the true characteristics (see Figure 1.a). In this case, our characteristics originate at points (x,t^{n+1}) and are given by $Y(\theta;x,t^{n+1})$ in Ω_1 and Ω_2. In Ω_3, the characteristics originate at points (b,t) on the outflow boundary and are given by $Y(\theta;b,t)$. The notation introduced in Section 2 for exact tracking is also used in our numerical scheme formulation, however we modify it for this approximate characteristic tracking. Accordingly, we define $\tilde{x}$ satisfying $x = Y(t^n;\tilde{x},t^{n+1})$ and $x^* = Y(t^n;x,t^{n+1})$ as the head and the foot respectively, of the Runge-Kutta approximate characteristics. The foot of a characteristic with head on the outflow boundary is denoted by $b^*(t) = Y(t^n;b,t)$ for $t \in [t^n,t^{n+1}]$. We also define $t^*(x)$ (given by the relation $a = Y(t^*(x);x,t^{n+1})$) as the exit

time of the characteristic $Y(\theta; x, t^{n+1})$ at the inflow boundary. On the other hand $\tilde{t}(x)$ (given by $x = Y(t^n; b, \tilde{t}(x))$) is such that the point $(b, \tilde{t}(x))$ on the outflow boundary backtracks to the point (x, t^n). The two time increments $\Delta t^{(I)}(x)$ and $\Delta t^{(O)}(x)$ are as defined before in (2.12).

The reference equation using this approximate characteristic tracking is derived in a similar manner as was done for equation (2.23). Since, however, the solution of u at time level t^{n+1} is sensitive to errors arising from the evaluation of the terms of (2.23) which involve integrals of the trial function $U(\cdot, t^n)$ at the previous time level, these terms must be treated with care. That these integrals are difficult to evaluate (especially in higher dimensions) is due to the fact that the test functions are defined by extending back along the approximate characteristics their values from time t^{n+1} and may be substantially distorted by this process [3, 45, 53]. To indicate the possible complications that may arise, we note that quite complicated geometries may occur even in the case of a constant velocity field. For example, when the support of a test function in three dimensions is traced back in time and intersects a boundary of the spatial domain, a four dimensional space-time region with a complicated geometry results as the support of the space-time test function.

The backtracking scheme uses the approximate characteristic Y to change variables in each of the integrals where the test functions are evaluated at time level t_+^n. In this way, the integrals are rewritten as integrals at time t^{n+1} (or, as the case may be, at the outflow boundary) of test functions (i.e. hat functions on the grid) at the current time integrated against trial functions evaluated at the foot of the characteristics. The term 'backtracking' comes from the use of the backward characteristics to determine the trial function values at the previous time. Hence after some rearrangement and combining of terms, the reference equation of the piecewise linear trial functions U using Runge-Kutta backward tracking is given by

$$\begin{aligned}
&\int_a^b U(x,t^{n+1})\, w(x,t^{n+1})\, dx + \int_a^{\tilde{a}} \Delta t^{(I)}(x)\, (DU_x)(x,t^{n+1})\, w_x(x,t^{n+1})\, dx \\
&\qquad + \int_{\tilde{a}}^b \frac{\Delta t}{2} \Big((DU_x)(x,t^{n+1}) \;+\; (DU_{x^*})(x^*,t^n) \Big)\; w_x(x,t^{n+1})\, dx \\
&\qquad + \int_{t^n}^{t^{n+1}} (VU - DU_x)(b,t)\, w(b,t)\, dt - \int_{t^n}^{t^{n+1}} (VU - DU_x)(a,t)\, w(a,t)\, dt \\
&\qquad - \int_{t^n}^{t^{n+1}} \frac{(t-t^n)}{2} \Big((DU_x)(b,t) \;+\; (DU_{x^*})(b^*(t),t^n) \Big)\; w_t(b,t)\, dt \\
&= \int_{\tilde{a}}^b Y_x(t^n; x, t^{n+1})\, U(x^*,t^n)\, w(x,t^{n+1})\, dx - \int_{t^n}^{t^{n+1}} Y_t(t^n; b, t)\, U(b^*(t),t^n)\, w(b,t)\, dt \\
&\qquad + \int_a^b \frac{\Delta t^{(I)}(x)}{2} \Big(f(x,t^{n+1}) \;+\; Y_x(t^*(x); x, t^{n+1})\, f(x^*,t^*(x)) \Big)\; w(x,t^{n+1})\, dx \\
&\qquad + \int_{t^n}^{t^{n+1}} \frac{(t-t^n)}{2} \Big(V(b,t)\, f(b,t) - Y_t(t^n; b, t)\, f(b^*(t),t^n) \Big)\, w(b,t)\, dt,
\end{aligned} \tag{3.5}$$

where in the third integral on the right hand side, x^* is a on $(a, \tilde{a})$. This general reference equation holds for all nodes $x_i, (i = 0, \ldots, I)$ and $t_i,\ (i = I, \ldots, I + IC)$, and simplifies in specific cases. The stiffness matrix is updated by evaluating terms involving U at time level

t^{n+1} and at the outflow boundary in equation (3.5). Likewise, by evaluating the remaining terms, we can update the right hand side vector of the generated system.

As we mentioned earlier, one difficulty arises in accurately computing the terms evaluated at feet of characteristics (i.e. x^* or $t^*(x)$), since several grid points from the previous time level may occur as backtracked points within a given interval at the current time. To illustrate how to overcome this difficulty, we will focus on the first term on the right hand side of equation (3.5) applied with test function w_i. In this case, when x varies over the interval $[x_{i-1}, x_i]$ (i.e., the left half of the support of $w_i(\cdot, t^{n+1})$), x^* will vary over the interval $[x_{i-IC-3}, x_{i-IC}]$. Therefore, due to the distortion by the characteristic tracking, $U(x^*, t^n)$ is not a piecewise linear function, but rather a piecewise smooth function of $x \in [x_{i-1}, x_i]$. This possible loss of smoothness, however, affects the accuracy of high order quadrature methods. Therefore, we simply subdivide the interval so that $U(x^*, t^n)$ is smooth on each subinterval and apply numerical integration to each subinterval separately. To illustrate the idea, we suppose x^*_{i-1} is in $[x_{j-1}, x_j)$ and x^*_i belongs to $[x_{j+1}, x_{j+2})$, then we would split the integral into three parts along the intervals $(x_{i-1}, \tilde{x}_j)$, $[\tilde{x}_j, \tilde{x}_{j+1})$, and $[\tilde{x}_{j+1}, x_i)$. Newton iteration is applied to determine the points at the current time level that track back to the grid points at the previous time level. (Recall that approximate Runge-Kutta forward tracking and back tracking may not be inverse operations for variable velocity fields). Once these intervals are determined, we may numerically integrate by determining quadrature points in each subinterval and then backtracking them to perform the quadrature with values of the trial function. The amount of piecewise smoothness will be determined by the corresponding smoothness of the velocity field. Additional information on this general problem and how to treat multivariate problems may be found in [28, 38, 52].

Another difficulty in incorporating the known values of the trial function in equation (3.5) arises from evaluating the expression $U_{x^*}(x^*, t^n)$ when x^* happens to be one of the nodal points $\{x_i\}_{i=0}^I$ at which U_{x^*} may have a jump discontinuity. Since our characteristic tracking is only approximate, we assume that all points within a small tolerance of x_i belong to the interval (x_i, x_{i+1}). This introduces an error which is controlled to within the desired order provided the tolerance is of the same order.

The scheme for nodes near the inflow boundary (i.e., x_i $(i = 0, ...IC + 1)$) differs since the characteristics traced back strike that boundary and lead to boundary terms appearing in the scheme. In the case of Robin flux boundary condition, we can easily change the fifth integral on the left side of equation (3.5) as follows

$$\int_{t^n}^{t^{n+1}} (VU - DU_x)(a, t)\, w(a, t)\, dt = \int_{t^n}^{t^{n+1}} g_3(t)\, w(a, t)\, dt. \tag{3.6}$$

Dirichlet inflow boundary condition introduces extra difficulty, since then the unknown diffusive flux term in the fifth integral on the left side of equation (3.5) appears in the scheme equations for nodes $x_i < \tilde{a}$. An alternative treatment for the diffusion term discussed in [44, 52] avoids this difficulty. Instead of integrating the term $\int_{t^n}^{t^{n+1}} -(Du_x)_x\, w\, dxdt$ by parts as we did in the derivation of the variational formulation (2.4) and then applying the integral approximation (trapezoidal, Euler), we can reverse the order, whence we get the term

$$\int_a^{\tilde{a}} \frac{d\Delta t^{(I)}(x)}{dx} (DU_x)(x, t^{n+1})\, w(x, t^{n+1})\, dx \tag{3.7}$$

instead of the diffusive flux in the fifth term on the left side of (3.5). The fifth term on the left side of (3.5) then simplifies to

$$\int_{t^n}^{t^{n+1}} V(a,t)\; g_1(t)\; w(a,t)\; dt. \tag{3.8}$$

Since the value of the trial function U is known at node x_0 from the prescribed Dirichlet boundary condition, we don't need to formulate equations there. Hence our scheme will be stipulated only for nodes x_i $(i = 1, \ldots, I)$. However, we do modify $w_1 = w_0 + w_1$ so that the test functions sum to one in order to maintain mass conservation.

Neumann inflow boundary condition generates a more natural scheme in the sense that a trapezoidal approximation, instead of the backward Euler approximation described above, can be implemented for the diffusive integral over Ω_1. The advantage of this treatment is that it symmetrizes the inflow terms thus maintaining the symmetry of the whole formulation. Implementing this boundary condition leads to the following two changes to equation (3.5): (i) a factor of $1/2$ multiplies the second integral on the left side, and (ii) the additional term of

$$-\int_a^{\tilde{a}} \frac{\Delta t^{(I)}(x)}{2} g_2(t^*(x))\; w_x(x, t^{n+1})\; dx \tag{3.9}$$

is added on the left side. The fifth term on the left side of equation (3.5) is replaced by

$$\int_{t^n}^{t^{n+1}} (VU)(a,t)\; w(a,t)\; dt + \int_{t^n}^{t^{n+1}} g_2(t)\; w(a,t)\; dt. \tag{3.10}$$

Wang, Ewing, and Russell [52] describe in detail several possible ways to treat the first integral in equation (3.10). Their findings suggest combining this term with the first term on the left hand side of the reference equation (3.5) and replacing these with the term

$$\int_{\tilde{a}}^{b} U(x, t^{n+1})\; w(x, t^{n+1}) dx. \tag{3.11}$$

Although this term is not exact for a variable velocity filed V, the error introduced is within the desired order.

Due to the fact that we generate unknowns at the outflow boundary at nodes t_i, boundary treatment here becomes very important. First we note that $U(b, t^n)$ is known from the previous time step solution, hence, we don't impose an equation at $t_{I+IC} = t^n$. Therefore, as we did earlier in the case of Dirichlet inflow conditions, we redefine the test function $w_{I+IC-1} := w_{I+IC-1} + w_{I+IC}$, to maintain mass balance. For test functions w_i, $(i = I + 1, \ldots, I + IC - 1)$, the terms on the inflow boundary and terms evaluated at time t^{n+1} of equation (3.5) vanish. Thus for nodes t_i $(i = I + 1, \ldots, I + IC - 1)$, the reference equation (3.5) simplifies to the following

$$\begin{aligned}
&\int_{t^n}^{t^{n+1}} (VU - DU_x)(b,t)\; w_i(b,t)\; dt \\
&\qquad - \int_{t^n}^{t^{n+1}} \frac{(t - t^n)}{2} \Big((DU_x)(b,t) \;+\; (DU_{x^*})(b^*(t), t^n) \Big)\; w_{it}(b,t)\; dt \\
&= \; - \int_{t^n}^{t^{n+1}} Y_t(t^n; b, t)\; U(b^*(t), t^n)\; w_i(b,t)\; dt \\
&\qquad + \int_{t^n}^{t^{n+1}} \frac{(t - t^n)}{2} \Big(V(b,t)\; f(b,t) \;-\; Y_t(t^n; b, t) f(b^*(t), t^n) \Big)\; w_i(b,t)\; dt.
\end{aligned} \tag{3.12}$$

We describe below how this equation changes for all three types of outflow boundary conditions. The equation for node x_I, has in addition to the terms in (3.12) some other terms that are in equation (3.5) which don't vanish for this node. Neumann outflow boundary condition can be incorporated in equation (3.12), simply by making the change $-(DU_x)(b,t) = h_2(t)$ in the first and second integrals on the left hand side of this equation. Similarly the flux outflow condition can be incorporated in equation (3.12) by applying the condition to the first integral on the left hand side, and using the relation $-(DU_x)(b,t) = h_3(t) - (VU)(b,t)$ for the second integral on the left hand side of equation (3.12). In the case of outflow Dirichlet condition, the solution $U(b,t^{n+1})$ is known from the boundary condition, therefore the equations for $i \leq I-1$ decouple and can be solved for $U(x_i,t^{n+1}),\ (i=0...I-1)$. Unless we desire the values of the derivative of the solution at the outflow boundary, we don't generate any equations there.

3.2 Forward Tracking Scheme

In this brief section we indicate the development of a scheme (FRKC) based on a 'forward tracking' which is a feasible alternative for the backward tracking scheme of the last subsection especially for multidimensional problems. With the test functions as defined earlier by equations (3.3)–(3.4), we use the reference equation (2.23) to derive the numerical scheme for Runge-Kutta forward tracking. Here again we wish to avoid the expensive task of backtracking the geometry to perform the integration of the test functions at the previous time level. Instead we perform this integration by using the fixed spatial grid of the trial function at $t = t^n$ and apply numerical quadrature. The values of the test function required by the quadrature are obtained by forward tracking the quadrature points and evaluating $w_i(\tilde{x},t^{n+1})$ or its derivatives at time t^{n+1}. This forward scheme is only used to evaluate certain terms to incorporate known values and therefore does not lead to distorted grids that comprise a major drawback of explicit numerical schemes.

In this scheme, the characteristics originate at points (x,t^n) and are given by $Y(\theta;x,t^n)$ in Ω_2 and Ω_3 or they originate at points (a,t) and are given by $Y(\theta;a,t)$ in Ω_1. Here again we use the same notation established in Sections 2 and 3, except we redefine them for this particular forward tracked approximate characteristics. Accordingly, we define $\tilde{x} = Y(t^{n+1};x,t^n)$ and x^* satisfying $x = Y(t^{n+1};x^*,t^n)$ as the head and foot of the approximate characteristic. Moreover, we let $t^*(x)$ (given by $x = Y(t^{n+1};a,t^*(x))$) and $\tilde{t}(x)$ (given by $b = Y(\tilde{t}(x);x,t^n)$) denote the exit time of the approximate characteristics at the inflow and outflow boundaries, respectively. The time increments $\Delta t^{(I)}$ and $\Delta t^{(O)}$ are then given by equation (2.12), where $t^*(x)$ and $\tilde{t}(x)$ extend to t^n and t^{n+1}, respectively, if they are defined by characteristics in Ω_2. The reference equation for the forward scheme, derived in a similar manner as equation

(2.23), is given by

$$
\begin{aligned}
&\int_a^b U(x,t^{n+1})\, w(x,t^{n+1})\, dx + \int_a^{\tilde{a}} \Delta t^{(I)}(x)\, (DU_x)(x,t^{n+1})\, w_x(x,t^{n+1})\, dx \\
&\quad + \int_{\tilde{a}}^b \frac{\Delta t}{2} (DU_x)(x,t^{n+1})\, w_x(x,t^{n+1})\, dx \\
&\quad + \int_a^b \frac{\Delta t^{(O)}(x)}{2}\, (DU_x)(x,t^n)\, w_x(x,t^n_+)\, dx - \int_{t^n}^{t^{n+1}} \frac{(t-t^n)}{2} (DU_x)(b,t)\, w_t(b,t)\, dt \\
&\quad + \int_{t^n}^{t^{n+1}} (VU - DU_x)(b,t)\, w(b,t)\, dt - \int_{t^n}^{t^{n+1}} (VU - DU_x)(a,t)\, w(a,t)\, dt \\
= &\quad \int_a^b U(x,t^n)\, w(x,t^n_+)\, dx + \int_{t^n}^{t^{n+1}} \frac{(t^{n+1}-t)}{2} V(a,t)\, f(a,t)\, w(a,t)\, dt \\
&\quad - \int_{t^n}^{t^{n+1}} \frac{(t-t^n)}{2} Y_t(t; b^*(t), t^n)\, f(b,t)\, w(b,t)\, dt \\
&\quad + \int_a^b \frac{\Delta t^{(I)}(x)}{2} f(x,t^{n+1})\, w(x,t^{n+1})\, dx + \int_a^b \frac{\Delta t^{(O)}(x)}{2} f(x,t^n)\, w(x,t^n_+)\, dx,
\end{aligned}
\tag{3.13}
$$

The boundary treatment is similar to that of the backtracking scheme BRKC.

3.3 Experimental Order of Convergence

In this subsection we establish numerically the order of convergence of the two schemes developed for equation (2.1) as well as the backward Euler ELLAM [52], referred to as BE-ELLAM. The test problem involves the transport of a Gaussian distribution (described in Section 5.1) initially centered at zero. The spatial domain is $[0, 1.4]$ with a temporal domain $[0, 1]$. In this test we choose the small diffusion coefficient of $D = 10^{-4}$, and consider the two velocity fields: $V = 1 + 0.1x$ and the more rapidly changing $V = 1 - 0.5x$. The right hand side in equation (2.1) is generated from this data and the analytical solution. The L_2 and L_1 norms of the residual error of the solution U of all three schemes are given by

$$
\max_{n=0,..,N} \|U(x,t^n) - u(x,t^n)\|_{L^p(a,b)} \le C_\alpha (\Delta x)^\alpha + C_\beta (\Delta t)^\beta, \quad p = 1, 2
$$

where α, β give the order of convergence of the error in space and time respectively, and C_α, C_β are positive constants. To obtain the order of convergence in space we fix $\Delta t = 1/500$ to insure time truncation errors are appropriately small. We then perform runs varying Δx and apply a linear regression on the L_p $(p = 1, 2)$ norms of the error to determine the parameter α. Tables 1 and 3 present the results of these runs and the computed value of the parameter α for the two velocity fields described above. In a similar manner we fix $\Delta x = 1/700$ and perform runs varying Δt to estimate the value of the parameter β. Tables 2 and 4 give corresponding results for β for the two velocity fields. From these results we clearly see that the two schemes developed are corroborated to be second order in space and time. We also see that BE-ELLAM, as was expected, is second order in space but only first order in time. The orders are more apparent in the rapidly changing velocity field $V = 1 - 0.5x$ (Tables 3 and 4). Tables 1 and 3 show that when the time step Δt is very small, the BRKC, FRKC, and BE-ELLAM schemes generate solutions with comparable errors. This is expected since all the schemes are second-order accurate in space and the temporal errors are negligible. In

practice one wishes to use largest possible time step in numerical simulations to enhance the efficiency without sacrificing accuracy. Therefore, Tables 2 and 4 bear more computational aspect since very large time steps are normally desired. One sees that the BRKC and FRKC schemes further reduce the temporal errors in BE-ELLAM, which are themselves significantly smaller than most Eulerian methods. This justifies the appropriateness of these schemes when large time steps are to be taken. The constant C_β is much smaller than C_α for all three schemes corroborating that time truncation errors are smaller that spatial errors, a strong advantage of characteristic methods in general.

4 Description of Some Other Methods

The necessity to numerically solve advection-dominated advection-diffusion equation with high accuracy has lead to the development of many specialized methods. In this section we briefly describe some well perceived methods which are widely used in practice. In the next section we carry out experiments to compare the performance of the BRKC and FRKC schemes with these methods. In this description, we impose all the assumptions on the velocity field $V(x,t)$ and the diffusion coefficient $D(x,t)$ which were described in Section 2 and describe the methods with Dirichlet boundary conditions.

4.1 Galerkin and Petrov-Galerkin finite element methods

The linear Galerkin (GAL), quadratic Petrov-Galerkin (QPG), and cubic Petrov-Galerkin (CPG) FEM methods with a Crank-Nicholson time discretization and Dirichlet inflow and outflow boundary conditions for equation (2.1) are described by the following formulation

$$\begin{aligned}
&\int_a^b U(x,t^{n+1})w_i(x)dx - \int_a^b \frac{\Delta t}{2}\left(VU - DU_x\right)(x,t^{n+1})\, w_{ix}(x)dx \\
&= \int_a^b U(x,t^n)w_i(x)dx - \int_a^b \frac{\Delta t}{2}\left(VU - DU_x\right)(x,t^n)w_{ix}(x)dx \\
&\quad + \int_a^b \frac{\Delta t}{2}\Big(f(x,t^{n+1}) + f(x,t^n)\Big)\, w_i(x)dx
\end{aligned} \tag{4.1}$$

where the trial function $U(x,t^{n+1})$ is piecewise linear on the intervals defined by the partition. The three methods differ in their choices of the test functions $w_i(x)$ $(i = 1, 2, \ldots I-1)$. In the GAL method, the test functions are chosen from the space of the trial functions, thus, $w_i(x)$ are the hat functions defined by equation (3.3) where $w_i(x)$ replaces $w_i(x,t^{n+1})$. The Petrov-Galerkin methods were designed to improve the GAL method by introducing some upwinding in the test space. The QPG methods use test functions, which are the sum of the standard hat functions and quadratic asymmetric perturbation terms, defined by

$$w_i(x) = \begin{cases} \dfrac{(x-x_{i-1})}{\Delta x_i} + 3\,\alpha_i \dfrac{(x-x_{i-1})(x_i-x)}{\Delta x_i^2}, & x \in [x_{i-1}, x_i], \\ \dfrac{(x_{i+1}-x)}{\Delta x_{i+1}} - 3\alpha_{i+1}\dfrac{(x-x_i)(x_{i+1}-x)}{\Delta x_{i+1}^2}, & x \in [x_i, x_{i+1}], \\ 0 & \text{otherwise}, \end{cases} \tag{4.2}$$

where the parameter $\alpha_i = \coth(\frac{V_i \Delta x_i}{2D_i}) - \frac{2D_i}{V_i \Delta x_i}$ with V_i and D_i being the arithmetic mean of the velocity field and the diffusion coefficient over the interval (x_{i-1}, x_i). The CPG methods on the other hand use test functions which have symmetric cubic perturbation terms added to the hat functions as follows,

$$w_i(x) = \begin{cases} \dfrac{(x - x_{i-1})}{\Delta x_i} + 5\,\gamma_i \dfrac{(x - x_{i-1})(x_i - x)(x_{i-1} + x_i - 2x)}{\Delta x_i^3}, & x \in [x_{i-1}, x_i], \\ \dfrac{(x_{i+1} - x)}{\Delta x_{i+1}} - 5\gamma_{i+1} \dfrac{(x - x_i)(x_{i+1} - x)(x_i + x_{i+1} - 2x)}{\Delta x_{i+1}^3}, & x \in [x_i, x_{i+1}], \\ 0 & \text{otherwise}, \end{cases} \quad (4.3)$$

where $\gamma_i = {Cr_i}^2$, with $Cr_i = \frac{V_i \Delta t}{\Delta x_i}$ is the Courant number averaged over the interval (x_{i-1}, x_i). Although many other Petrov-Galerkin formulations are also known to solve equation (2.1) reasonably well, QPG and CPG methods are among the most popular ones in practice.

4.2 The Streamline Diffusion FEM methods

The Streamline Diffusion method (SDM) is applied to the non-conservative form of equation (2.1) given by

$$\mathcal{L}u \equiv u_t + V(x,t)u_x + V_x(x,t)u - (D(x,t)u_x)_x = f(x,t). \quad (4.4)$$

Here we describe the linear SDM formulation for this equation. We divide the domain into the time slabs $[a,b] \times (t^n, t^{n+1}]$, and successively on each slab, we seek a continuous and piecewise linear function $U(x,t)$ (discontinuous in time at t^n and t^{n+1}) which satisfies the following formulation,

$$\begin{aligned} \int_{t^n}^{t^{n+1}} \int_a^b \left[U_t + VU_x + V_x U\right] \left[w + \delta(w_t + V w_x)\right] dxdt + \int_{t^n}^{t^{n+1}} \int_a^b DU_x\, w_x dxdt \\ -\delta \int_{t^n}^{t^{n+1}} \int_a^b (DU_x)_x \left(w_t + V w_x\right) dxdt + \int_a^b U_+^n w_+^n dx \\ = \int_{t^n}^{t^{n+1}} \int_a^b f \left[w + \delta(w_t + V w_x)\right] dxdt + \int_a^b U_-^n w_-^n dx. \end{aligned} \quad (4.5)$$

The test function w is piecewise linear in both space and time (bilinear) in the slab, and is discontinuous at time t^n and t^{n+1} and is zero at $x = a$ and $x = b$. In equation (4.5) $w_\pm^n = \lim_{t \to (t^n)^\pm} w(x,t)$, $U_-^0 = u_o(x)$, and δ is a free parameter, described below, that has significant influence on the accuracy of the scheme. There are many relations that can be used for the parameter δ. One of the most widely used relations is $\delta = C\frac{h}{\sqrt{1+V^2}}$, where h is the mesh diameter and C is a constant to be chosen [35]. The choice of C determines the amount of diffusion applied in the direction of the characteristics and therefore has a great effect on the accuracy of the scheme. One requires that C is large enough to produce non-oscillatory solution, but not too large to damp the solution. This choice is, in general, problem dependent and not clear in practice. Although there are more improved versions of SDM method with shock capturing capacity which produce better approximations, they usually have nonlinear formulations (even though they model linear equations), have more free parameters similar to δ (described above) that need to be chosen carefully, and also have higher computational cost. The formulation (4.5) is the one we chose for numerical experiments described in the next section.

4.3 The Continuous and Discontinuous Galerkin FEM methods

The Continuous and Discontinuous Galerkin methods (CGM and DGM) [42, 43] apply to the non-conservative form of equation (2.1) given by equation (4.4). The domain $\Omega_g = (a,b) \times (0,T)$ is divided into a quasi-uniform triangulation with side length h, and Dirichlet data is assumed on the inflow portion of the boundary denoted by $\Gamma_{(I)}$ and given by $\mathbf{V}(x,t) \cdot \mathbf{n} < 0$, where $\mathbf{V}(x,t) = (V(x,t), 1)$ gives the characteristic direction and $\mathbf{n} = (n_1, n_2)$ is the outward unit normal vector. The boundary data given at the outflow portion of the boundary are not used in the formulation. In the DGM method one seeks a discontinuous approximation $U(x,t)$, which lies in the space $P_n(\mathcal{T})$ of polynomials of degree at most n on each triangle $\mathcal{T}$, and satisfies the equation

$$\begin{aligned}\int_{\mathcal{T}} (U_t + VU_x + V_x U)\, w\, dxdt - \int_{\Gamma_{(I)}(\mathcal{T})} U^+\, w\mathbf{V}\cdot\mathbf{n}\, dS + \int_{\Gamma^*_{(I)}(\mathcal{T})} DU_x^+ w\, n_1\, dS \\ = \int_{\mathcal{T}} f w\, dxdt - \int_{\Gamma_{(I)}(\mathcal{T})} U^-\, w\mathbf{V}\cdot\mathbf{n}\, dS + \int_{\Gamma^*_{(I)}(\mathcal{T})} DU_x^- w\, n_1\, dS, \quad \text{for all } w \in P_n(\mathcal{T})\end{aligned} \tag{4.6}$$

where $\Gamma^*_{(I)}(\mathcal{T})$ is the inflow boundary of $\mathcal{T}$ exclusive of any sides on the boundary of the domain, $U^{\pm}(x,t) \equiv \lim_{\varepsilon\to 0^+} U((x,t) \pm \varepsilon\mathbf{V})$, and U^- is the solution at the previous element or an interpolation of the prescribed Dirichlet data for sides on $\Gamma_{(I)}$. CGM is formulated in the same way by requiring a solution $U(x,t) \in P_n(\mathcal{T})$ which satisfies equation (4.6), however there are two main differences: First, the trial function $U(x,t)$ is required to be continuous over the domain Ω_g, and the test functions are in $P_{n-\rho(\mathcal{T})}(\mathcal{T})$, where $\rho(\mathcal{T})$ is the number of inflow sides that $\mathcal{T}$ has. Secondly, the continuity requirement in CGM makes the second terms on both sides of (4.6) cancel each other. In both of these methods, one iterates over the elements solving a linear system of order equal to the degree of freedom on each element which makes these schemes quasi-explicit. In the next section, we consider the lowest-order CGM ($n = 2$), and DGM ($n = 1$).

4.4 High Resolution Methods (MUSCL and ENO)

High resolution methods from computational fluid dynamics are known to be good for purely hyperbolic equations. An extension of these methods to equation (2.1) is based on time-splitting of the equation, as described below, and then a high-order Godunov method can be used to solve the advective part, with a mixed FEM method to solve the diffusive part [16]. We consider two such schemes, the first based on Monotone Upstream-centered Scheme for Conservation Laws (MUSCL) which was developed by van Leer [49], and a second, based on a generalization of the first, called the Essentially Non-Oscillatory scheme (ENO) which was developed by Harten et al. [27, 46]. Assuming that $U^n(x)$ approximates the solution $u(x,t^n)$ of equation (2.1), we can generate an approximation of $u(x,t^{n+1})$ as follows: First the MUSCL or ENO scheme, described below, can be applied to find a solution of the advective equation

$$\begin{aligned} \bar{u}_t + (V\bar{u})_x &= 0, && \text{for } (x,t) \in [a,b] \times (t^n, t^{n+1}], \\ \bar{u}(x,t^n) &= U^n(x), && \text{for } x \in [a,b], \end{aligned} \tag{4.7}$$

which we denote $\bar{U}^{n+1}(x)$. Then the mixed method can be used to solve

$$\begin{aligned} u^*_t - (Du^*_x)_x &= f, && \text{for } (x,t) \in [a,b] \times (t^n, t^{n+1}], \\ u^*(x,t^n) &= \bar{U}^{n+1}(x), && \text{for } x \in [a,b] \end{aligned} \tag{4.8}$$

whose solution is the approximation $U^{n+1}(x)$ of $u(x,t^{n+1})$. We note the well-known fact that the mixed method in lowest-order approximation space and a trapezoidal rule of integration is equivalent to the block-centered finite difference scheme [21].

Now we describe the MUSCL and ENO schemes. Unlike the other methods discussed here which are node based, MUSCL and ENO are cell-centered based methods; i.e. the solution is approximated at the points $x_{i-1/2}\,(i = 1,\ldots,I)$, where $x_{i-1/2}$ is the mid point of the interval $[x_{i-1}, x_i]$. To simplify the presentation, we assume that the partition (2.2) is uniform. The MUSCL or ENO solution of equation (4.7) is given by

$$\bar{U}^{n+1}_{i-1/2} = U^n_{i-1/2} - \frac{\Delta t}{\Delta x}(V(x_{i-1/2},t^n)U^n_{i-1/2,L} - V(x_{i-\frac{3}{2}},t^n)U^n_{i-\frac{3}{2},L}), \tag{4.9}$$

where the Courant number is assumed not to exceed one (a stability requirement) and the left state $U^n_{i-1/2,L}$ is given by

$$U^n_{i-1/2,L} = \begin{cases} U^n_{i-1/2} + \dfrac{\Delta x}{2}\left(1 - V(x_{i-1/2},t^n)\dfrac{\Delta t}{\Delta x}\right)\delta U^n_{i-1/2}, & i = 1,\ldots,I, \\ g_1(t^n), & i = 0. \end{cases} \tag{4.10}$$

The two methods differ in the choice of the slope $\delta U^n_{i-1/2}$. The ENO formulation uses the slope given by

$$\delta U^n_{i-1/2} = \begin{cases} \Delta_+ U^n_{i-1/2}, & \text{if } |\Delta_+ U^n_{i-1/2}| \le |\Delta_- U^n_{i-1/2}|, \\ \Delta_- U^n_{i-1/2}, & \text{otherwise,} \end{cases} \tag{4.11}$$

where the difference operators are given by

$$\Delta_- U^n_{i-1/2} = \begin{cases} \dfrac{2(U^n_{i-1/2} - g_1(t^n))}{\Delta x}, & i = 1, \\ \dfrac{U^n_{i-1/2} - U^n_{i-3/2}}{\Delta x}, & i = 2,\ldots,I, \end{cases} \tag{4.12}$$

and

$$\Delta_+ U^n_{i-1/2} = \begin{cases} \dfrac{U^n_{i+1/2} - U^n_{i-1/2}}{\Delta x}, & i = 1,\ldots,I-1, \\ \dfrac{2(h_1(t^n) - U^n_{i-1/2})}{\Delta x}, & i = I. \end{cases} \tag{4.13}$$

The MUSCL formulation on the other hand uses the following definition for the slope

$$\delta U^n_{i-1/2} = \min\left\{\Delta_{lim} U^n_{i-1/2}, |\Delta_c U^n_{i-1/2}|\right\} \cdot \text{sgn}(\Delta_c U^n_{i-1/2}), \quad \text{for } i = 1,\ldots,I, \tag{4.14}$$

where sgn(x) = 1 for $x > 0$, sgn(x) = -1 for $x < 1$, and sgn(0) = 0,

$$\Delta_{lim} U^n_{i-1/2} = \begin{cases} \alpha_i \min\left\{|\Delta_+ U^n_{i-1/2}|, |\Delta_- U^n_{i-1/2}|\right\}, & \text{if } (\Delta_+ U^n_{i-1/2}) \cdot (\Delta_- U^n_{i-1/2}) > 0, \\ 0, & \text{otherwise,} \end{cases} \tag{4.15}$$

and

$$\Delta_c U^n_{i-1/2} = \begin{cases} \dfrac{U^n_{i+1/2} - 4g_1(t^n)}{3\Delta x}, & i = 1, \\ \dfrac{U^n_{i+1/2} - U^n_{i-3/2}}{2\Delta x}, & i = 2, \ldots, I-1, \\ \dfrac{4h_1(t^n) - U^n_{i-3/2}}{3\Delta x}, & i = I. \end{cases} \tag{4.16}$$

The parameter α_i in equation (4.15) is 2 for $i = 1, \cdots, I-1$ and 1 otherwise, which is the upper bound that allows the steeper representation of sharp fronts.

5 Numerical Experiments

In this section we describe numerical experiments which we use to compare the Runge-Kutta characteristic methods developed in this paper (using both forward- and back-tracking) with several generally well-regarded numerical schemes, including various Galerkin and Petrov-Galerkin finite element methods, high resolution methods in fluid dynamics, and the method of Streamline Diffusion. We apply these methods to two standard test problems (a smooth Gaussian distribution and a step function) for which we have analytic solutions to the advection-diffusion equation. In addition, each of these functions are typically used to test for numerical artifacts of proposed schemes, such as numerical stability and diffusion, spurious oscillations, phase errors, and Gibbs type effects near sharp fronts.

In order to test these proposed schemes for advection-dominated transport, we consider the model equation (2.1) over the time period $t \in [0, 1.0]$ with a variable velocity $V(x,t) = 1 + 0.1\,x$, and a relatively small diffusion coefficient of $D = 10^{-4}$. We consider both test problems for our initial/boundary conditions with the results for the Gaussian shown in figures beginning with label I and the step function with label II. For clarity of exposition, we have arranged the numerical methods into 5 groups based on common characteristics of their behavior and implementation. These groups are organized according to the following table:

Group	Methods
1	Runge-Kutta characteristic methods (BRKC and FRKC)
2	Crank-Nicholson FEM (Galerkin, Quadratic and Cubic Petrov-Galerkin)
3	Streamline Diffusion (with various selections of the control parameter).
4	Continuous and Discontinuous Galerkin
5	High resolution methods in fluid dynamics (MUSCL and ENO)

In our experiments, we have systematically varied the space and time steps to examine the performance of each method. For each grouping we have chosen to display 3 plots which provides a fair illustration of the accuracy of each method, their potential beneficial properties, as well as their possible undesirable numerical artifacts. For comparison to BRKC and FRKC, the first plot in each figure, labeled (a), presents the evolved solution for all methods in the group using a common space mesh ($\Delta x = 1/60$ for Problem I, $\Delta x = 1/100$ for Problem II) and a time step as close as possible to the BRKC/FRKC time step of $\Delta t = 1/10$, but chosen small enough to ensure stability. The third plot of the figure (labeled (c)) for each grouping shows the solutions with an optimally efficient and reasonable choice of space and time steps to produce a qualitatively comparable solution to that of the BRKC and FRKC schemes in Figures I.1 and II.1, respectively. The second plot in each Figure (labeled (b)) shows an intermediate stage for each grouping. For example, Figure I.2 consists of 3 plots ((a)-(c)) which shows the solutions for model problem I at time $T = 1.0$ for the methods in group 2 (spatial finite elements and a Crank-Nicholson time stepping) with $(\Delta x, \Delta t)$ taken as $(1/60, 1/69)$, $(1/60, 1/200)$, and $(1/100, 1/300)$, respectively. In this example, we were required by the CFL constraint to begin with $\Delta t = 1/69$, since the maximum velocity is 1.14 over the interval [0,1.4] and larger time steps result in unbounded solutions.

To gauge algorithm efficiency, we also compare the timings for each method to achieve the accuracy depicted in plot (c) of each figure. These results are presented in Tables 5-9, using the groupings of algorithms as we described in our list above. We realize, of course, that some code optimization may be possible but feel that these timings are representative of each scheme's efficiency on these model problems.

5.1 Model Problem I: Gaussian

Our first model problem is a Gaussian distribution over the spatial domain $[0, 1.4]$. We use baseline parameters of $\Delta x = 1/60$, $\Delta t = 1/10$ for each numerical scheme in our testbed and vary these parameters until we obtain results with errors comparable to the two Runge-Kutta methods (BRKC and FRKC). With the exception of the BRKC and FRKC schemes, each of these methods has implicit Courant restrictions on the time step which must be met for numerical solutions to be bounded and may not be chosen as large as that permitted by the ELLAM schemes.

Figure I.1 shows the initial condition for model problem I (plotted with solid line at the inflow boundary) along with the evolved solution at time $t = 1.0$. Near the right boundary, we see the analytic solution (solid line), the back-tracked BRKC solution (marker 'o'), and the forward-tracked FRKC solution (dotted line). Both methods use a spatial step of $\Delta x = 1/60$ with a relatively large time step of $\Delta t = 1/10$. Each of the two solutions give very accurate approximations which are free of numerical oscillations, artificial diffusion, phase error, and adverse boundary effects. The timings for the BRKC and FRKC schemes are presented in Table 5 and provide baseline timings for all experiments.

Figure I.2.a contains the plots of the analytic solution (solid line), the Galerkin approximation (labeled with symbol '+'), quadratic Petrov-Galerkin (dotted line) and cubic Petrov-Galerkin (labeled with symbol 'o') at time $t = 1.0$ with $\Delta x = 1/60$ where the time-stepping method employed is Crank-Nicholson. Due to Courant number restrictions on these

methods, an initial time step of $\Delta t = 1/69$ was required. This plot shows that there are significant trailing oscillations for both the Galerkin and quadratic Petrov-Galerkin methods and to a lesser extent for the cubic Petrov-Galerkin method. All methods in this group however have significant diffusion and a mild downstream phase error. As we decrease our mesh sizes to try to match the performance of the two Runge-Kutta characteristic schemes, we see in Figures I.2.b–I.2.c that the trailing oscillations and numerical diffusion are less pronounced (for all but the cubic Petrov-Galerkin method), but still persist for all three methods until we decrease Δx to $1/100$ and Δt to $1/300$. In this case the CPU requirement for these methods is two orders of magnitude larger than that required to achieve similar results using the BRKC or FRKC methods (see Table 6). In displaying the timings for these Crank-Nicholson schemes, we have presented, in the interest of space, only the average of the three schemes since the timings for each scheme was within one second of the other two methods.

Figure I.3 presents the corresponding results for the Streamline Diffusion Method. This method requires the use of a control parameter C, and we present in Figure I.3 the plots for three values of this parameter in each of the subplots (a)-(c). In Figure I.3.a we have used a time step of $\Delta t = 1/120$ which is the largest we may choose and have bounded solutions due to the method's Courant constraint. As Figure I.3 demonstrates, there are both leading and trailing oscillations, along with relatively strong numerical diffusion and a downstream phase error. These persist to a milder degree (see Figure I.3.c) as both the spatial and time steps are decreased. In Table 7 we present the timings for this method. For each selection of C, the CPU time is presented to compute the solution for $t = 1.0$. The timings for Figure I.3.a-c are at least 68.7, 269.1, and 402.1 seconds, respectively, which indicate a severe weakness of this method in certain applications. Another drawback of this method is that it is not clear in general how to choose the parameter C, which indicates that an iteration of this parameter may be necessary and the expense of this method will increase accordingly.

Figure I.4 presents the results for the Continuous (dotted line) and Discontinuous (labeled with symbol '+') Galerkin methods. Again due to Courant restrictions, we were able to take Δt no larger than $\Delta x = 1/60$. We see that there are significant leading and trailing oscillations and a mild phase error for these two schemes with the Discontinuous Galerkin method performing somewhat better of the two. However, this later method does exhibit some overshoot near the maximum of the Gaussian, which persists in plot (b) where $\Delta x = 1/120$ and $\Delta t = 1/180$. The accuracy of the two Runge-Kutta characteristic schemes are matched in plot (c) by taking $\Delta x = 1/180$ and $\Delta t = 1/180$, but both the CGM and DGM require a CPU expense of more than 120 seconds (see Table 8) as compared to 1.1 seconds for the FRKC and 2.1 seconds for the BRKC (see Table 5).

The final schemes which we wish to observe are the two high resolution methods in fluid dynamics (MUSCL and ENO) In Figure I.5, we have plotted the results of the simulation of these schemes where we again must take a relatively small initial time step of $\Delta t = 1/69$ due to the Courant restriction of these methods. The analytic solution is plotted as the solid line, while the ENO scheme uses a dotted line and the MUSCL scheme is plotted using the symbol '+'. The monotonicity of these methods is quite apparent, but there is a pronounced trailing non-negative oscillation as well as an overshoot near the peak of the pulse for both methods, with the ENO scheme producing the most overshoot. These

effects indicate strong mass balance errors for the Godunov schemes. Parts (b) and (c) of this figure, show that these artifacts persist until we reduce the mesh sizes to have values $\Delta x = 1/300$ and $\Delta t = 1/500$. Even with this reduction the trailing nonnegative oscillation is still apparent for both methods (see Figure I.5.c). To achieve this level of approximation required a total of 30.8 and 32.7 seconds of CPU time for the MUSCL and ENO schemes, respectively, which is a significant increase over the 1.1 sec required for the FRKC scheme, or for the BRKC (2.1 seconds).

5.2 Model Problem II: Step Function

In this section we discuss the corresponding experiments carried out above with the step function replacing the Gaussian distribution. The observations made from Problem I are still valid for all of the numerical schemes tested, but in this case there are several additional features we would like to point out which are less pronounced than in the case of a Gaussian distribution.

For this model problem our interval is $[0, 2]$ and we begin with $\Delta x = 1/100$. Figure II.1 shows the initial condition and analytic solution (solid line), together with the BRKC and FRKC solutions. We have taken $\Delta t = 1/10$ for these methods.

The Galerkin and Petrov-Galerkin methods with Crank-Nicholson time stepping (see Figure II.2) shows strong oscillations (both up- and down-stream) near each steep front. Figure II.3 shows that the streamline diffusion method exhibits a Gibbs' effect near each of the jump discontinuities in the initial function. In this case, it appears that reducing the value of C continues to improve the error, while in previous experiments [54], we have shown that the error may have local minimum as a function of C for this method. The Continuous and Discontinuous Galerkin methods (see Figures II.4 parts b-c) have a behavior very similar to the Streamline Diffusion method. This is to be expected since these methods are closely related. However, the Streamline Diffusion method has approximately double the unknowns which must be determined and is correspondingly more expensive to compute. The high resolution schemes (Figure II.5) tend to worsen slightly as the grids are refined past $\Delta x = 1/100$ and $\Delta t = 1/200$. Although the numerical error is somewhat high, the qualitative features of these solutions are good.

References

[1] J.W. Barrett and K.W. Morton, Approximate symmetrization and Petrov-Galerkin methods for diffusion-convection problems, Comp. Meth. Appl. Mech. Engrg. 45 (1984) 97–122.

[2] J.P. Benque and J. Ronat, Quelques difficulties des modeles numeriques en hydraulique, in: Glowinski and Lions, eds., Computing Methods in Applied Sciences and Engineering, (North-Holland, 1982) 471–494.

[3] P.J. Binning and M.A. Celia, A finite volume Eulerian-Lagrangian localized adjoint method for solution of the contaminant transport equations in two-dimensional multi-phase flow systems, Water Resour. Res. 32 (1996) 103–114.

[4] E.T. Bouloutas and M.A. Celia, An improved cubic Petrov-Galerkin method for simulation of transient advection-diffusion processes in rectangularly decomposable domains, Comp. Meth. Appl. Mech. Engrg. 91 (1991) 289–308.

[5] A. Brooks and T.J.R. Hughes, Streamline upwind Petrov-Galerkin formulations of convection dominated flows with particular emphasis on the incompressible Navier-Stokes equations, Comp. Meth. Appl. Mech. Engrg. 32 (1982) 199-259.

[6] M.A. Celia, I. Herrera, E. Bouloutas, and J.S. Kindred, A new numerical approach for the advective-diffusive transport equation, Numer. Methods Partial Differential Equations 5 (1989) 203–226.

[7] M.A. Celia, T.F. Russell, I. Herrera, and R.E. Ewing, An Eulerian-Lagrangian localized adjoint method for the advection-diffusion equation, Advances in Water Resources 13 (1990) 187–206.

[8] M.A. Celia and I.A. Ferrand, A comparison of ELLAM formulations for simulation of reactive transport in groundwater, in: Wang, ed., Advances in Hydro-Science and Engineering, Vol. 1(B) (University of Mississippi Press, 1993) 1829–1836.

[9] I. Christie, D.F. Griffiths, and A.R. Mitchell, Finite element methods for second order differential equations with significant first derivatives, Int. J. Num. Engrg. 10 (1976) 1389–1396.

[10] P. Colella, A direct Eulerian MUSCL scheme for gas dynamics, SIAM J. Sci. Stat. Comput. 6 (1985) 104–117.

[11] R.A. Cox and T. Nishikawa, A new total variation diminishing scheme for the solution of advective-dominant solute transport, Water Resour. Res. 27 (1991) 2645–2654.

[12] M.G. Crandall and A. Majda, Monotone difference approximations for scalar conservation laws, Math. Comp. 34 (1980) 1–21.

[13] H.K. Dahle, M.S. Espedal, R.E. Ewing, and O. Sœvareid, Characteristic adaptive subdomain methods for reservoir flow problems, Numer. Methods Partial Differential Equations 6 (1990) 279–309.

[14] H.K. Dahle, R.E. Ewing, and T.F. Russell, Eulerian-Lagrangian localized adjoint methods for a nonlinear advection-diffusion equation, Comput. Methods Appl. Mech. Engrg. 122 (1995) 223–250.

[15] C.N. Dawson, T.F. Russell, and M.F. Wheeler, Some improved error estimates for the modified method of characteristics, SIAM J. Numer. Anal. 26 (1989) 1487–1512.

[16] C.N. Dawson, Godunov-mixed methods for advective flow problems in one space dimension, SIAM J. Numer. Anal. 28 (1991) 1282–1309

[17] J. Douglas, Jr. and T.F. Russell, Numerical methods for convection-dominated diffusion problems based on combining the method of characteristics with finite element or finite difference procedures, SIAM J. Numer. Anal. 19 (1982) 871–885.

[18] B. Engquist and S. Osher, Stable and entropy satisfying approximations for transonic flow calculations, Math Comp. 34 (1980) 45–75.

[19] K. Eriksson and C. Johnson, Adaptive streamline diffusion finite element methods for stationary convection-diffusion problems, Math. Comp. 60 (1993) 167–188.

[20] M.S. Espedal and R.E. Ewing, Characteristic Petrov-Galerkin subdomain methods for two-phase immiscible flow, Proceedings of the first world congress on computational mechanics (Austin, Tex., 1986), Comput. Methods Appl. Mech. Engrg. 64 (1987) 113–135.

[21] R.E. Ewing, ed., The Mathematics of Reservoir Simulation, Frontiers in Applied Mathematics, Vol. 1 (SIAM, Philadelphia, 1983).

[22] R.E. Ewing, Operator splitting and Eulerian-Lagrangian localized adjoint methods for multiphase flow, The mathematics of finite elements and applications, VII (Uxbridge, 1990), (Academic Press, London, 1991) 215–232.

[23] R. Falk and G.R. Richter, Local error estimates for a finite element method for hyperbolic and convection-diffusion equations, SIAM J. Numer. Anal. 29 (1992) 730-754.

[24] B.A. Finlayson, Numerical methods for problems with moving fronts, (Ravenna Park Publishing, Inc. Seattle, 1992).

[25] A.O. Garder, D.W. Peaceman, and A.L. Pozzi, Numerical calculations of multidimensional miscible displacement by the method of characteristics, Soc. Pet. Eng. J. 4 (1964) 26-36

[26] P. Hansbo and A. Szepessy, A velocity-pressure streamline diffusion finite element method for the incompressible Navier-Stokes equations, Comp. Meth. Appl. Mech. Engrg. 84 (1990) 107-129.

[27] A. Harten, B. Engquist, S. Osher, and S. Chakravarthy, Uniformly high order accurate essentially nonoscillatory scheme, III, J. Comput. Phys. 71 (1987) 231–303.

[28] R.W. Healy and T.F. Russel, A finite-volume Eulerian-Lagrangian localized adjoint method for solution of the advection-dispersion equation, Water Resour. Res. 29 (1993) 2399–2413.

[29] I. Herrera, R.E. Ewing, M.A. Celia, and T.F. Russell, Eulerian-Lagrangian localized adjoint method: the theoretical framework, Numer. Methods Partial Differential Equations 9 (1993) 431–457.

[30] J.M. Hervouet, Applications of the method of characteristics in their weak formulation to solve two-dimensional advection-equations on mesh grids, in: Taylor et al., (eds.), Computational Techniques for Fluid Flow, Vol. 5 of Recent Advances in Numerical Methods in Fluids (Pineidge Press, 1986) 149–185.

[31] T.J.R. Hughes, and A.N. Brooks, A multidimensional upwinding scheme with no crosswind diffusion, in: Hughes, ed., Finite Element Methods for Convection Dominated Flows 34 (ASME, New York, 1979).

[32] T.J.R. Hughes and M. Mallet, A new finite element formulation for computational fluid dynamics III, The general Streamline operator for multidimensional advective-diffusive systems, Comp. Meth. Appl. Mech. Engrg. 58 (1986) 305–328.

[33] T.J.R. Hughes, Multiscale phenomena: Green functions, the Dirichlet-to-Neumann formulation, subgrid scale models, bubbles, and the origins of stabilized methods, Comp. Meth. Appl. Mech. Engrg. 127 (1995) 387–401.

[34] C. Johnson and J. Pitkäranta, An analysis of discontinuous Galerkin methods for a scalar hyperbolic equation, Math. Comp. 46 (1986) 1–26.

[35] C. Johnson, Numerical solution of partial differential equations by the finite element method, Cambridge University Press (Cambridge, 1987).

[36] C. Johnson, A. Szepessy, and P. Hansbo, On the convergence of shock-capturing streamline diffusion finite element methods for hyperbolic conservation laws, Math. Comp. 54 (1990) 107–129.

[37] P. Lesaint and P.A. Raviart, On a finite element method for solving the neutron transport equation, in: C. DeBoor, ed., Mathematics Aspects of Finite Elements in Partial Differential Equations (Academic Press, 1974) 89–123.

[38] K.W. Morton, A. Priestley, and E. Süli, Stability of the Lagrangian-Galerkin method with nonexact integration, RAIRO Modél. Math. Anal. Numér. 22 (1988) 123-151.

[39] S.P. Neuman, An Eulerian-Lagrangian numerical scheme for the dispersion-convection equation using conjugate space-time grids, J. Comput. Phys. 41 (1981) 270–294.

[40] G.F. Pinder and H.H. Cooper, A numerical technique for calculating the transient position of the saltwater front, Water Resour. Res. (1970) 875–882.

[41] O. Pironneau, On the transport-diffusion algorithm and its application to the Navier-Stokes equations, Numer. Math. 38 (1982) 309–332.

[42] G.R. Richter, A finite element method for time dependent convection-diffusion equations, Math. Comp. 54 (1990) 81-106.

[43] G.R. Richter, The discontinuous Galerkin method with diffusion, Math. of Comp. 58 (1992) 631–643.

[44] T.F. Russell, Eulerian-Lagrangian localized adjoint methods for advection-dominated problems, in: Numerical analysis 1989 (Dundee, 1989), Pitman Res. Notes Math. Ser., 228, Longman Sci. Tech. (Harlow, 1990) 206–228.

[45] T.F. Russell and R.V. Trujillo, Eulerian-Lagrangian localized adjoint methods with variable coefficients in multiple dimensions, in: Gambolati, *et al.*, (eds.), Computational Methods in Surface Hydrology (Springer-Verlag, Berlin, 1990) 357–363.

[46] C. Shu and S. Osher, Efficient implementation of essentially non-oscillatory shock capturing schemes, J. Comput. Phys. 77 (1988) 439–471.

[47] P.K. Sweby, High resolution schemes using flux limiters for hyperbolic conservation laws, SIAM J. Numer. Anal. 28 (1991) 891-906.

[48] E. Tadmor, Numerical viscosity and the entropy condition for conservative difference schemes, Math. Comp. 43 (1984) 369–381.

[49] B. van Leer, On the relation between the upwind-differencing schemes of Godunov, Engquist-Osher and Roe, SIAM J. Sci. Statist. Comput. 5 (1984) 1–20.

[50] E. Varoglu and W.D.L. Finn, Finite elements incorporating characteristics for one-dimensional diffusion-convection equation, J. Comp. Phys. 34 (1980) 371–389.

[51] H. Wang, R.E. Ewing, and T.F. Russell, ELLAM for variable-coefficient convection-diffusion problems arising in groundwater applications, in: Russell *et al.* (eds.), Computational Methods in Water Resources IX, Vol. I, Computational Mechanics Publications and Elsevier Applied Science (London and New York, 1992) 25–31.

[52] H. Wang, R.E. Ewing, and T.F. Russel, Eulerian-Lagrangian localized adjoint methods for convection-diffusion equations and their convergence analysis, IMA Journal of Numerical Analysis 15 (1995) 405-459.

[53] H. Wang, R.C. Sharpley, and S. Man, An ELLAM scheme for advection-diffusion equations in multi-dimensions, in: Aldama *et al.*, (eds.), Computational Methods in Water Resources XI. Vol. II: Computational Mechanics Publications (Southampton and Boston, 1996) 99 – 106.

[54] H. Wang, M.A. Al-Lawatia, and A.S. Telyakovskiy, A Runge-Kutta Characteristic Method for First-Order Linear Hyperbolic Equations (to appear).

[55] J.J. Westerink and D. Shea, Consider higher degree Petrov-Galerkin methods for the solution of the transient convection-diffusion equation, Int. J. Numer. Meth. Engrg. 28 (1989) 1077-1101.

[56] M.F. Wheeler and C.N. Dawson, An operator-splitting method for advection-diffusion-reaction problems, The mathematics of finite elements and applications, VI (Uxbridge, 1987), (Academic Press, London-New York, 1988) 463–482.

Method	Δt	Δx	L_2 Error	L_1 Error
BRKC	1/500	1/40	1.708301×10^{-2}	1.008468×10^{-2}
	1/500	1/50	9.762816×10^{-3}	5.012535×10^{-3}
	1/500	1/60	6.028822×10^{-3}	2.822963×10^{-3}
	1/500	1/70	3.989709×10^{-3}	1.738832×10^{-3}
	1/500	1/80	2.793234×10^{-3}	1.191840×10^{-3}
			$\alpha = 2.6181$	$\alpha = 3.0979$
			$C_\alpha = 270.4686$	$C_\alpha = 919.3184$
FRKC	1/500	1/40	3.280644×10^{-2}	1.560330×10^{-2}
	1/500	1/50	2.993149×10^{-2}	1.335517×10^{-2}
	1/500	1/60	2.290385×10^{-2}	1.005026×10^{-2}
	1/500	1/70	1.415099×10^{-2}	6.052967×10^{-3}
	1/500	1/80	5.040757×10^{-3}	2.071540×10^{-3}
			$\alpha = 2.4812$	$\alpha = 2.6757$
			$C_\alpha = 418.3782$	$C_\alpha = 405.2484$
BE-ELLAM	1/500	1/40	1.727842×10^{-2}	1.019763×10^{-2}
	1/500	1/50	1.004383×10^{-2}	5.125955×10^{-3}
	1/500	1/60	6.370859×10^{-3}	2.974945×10^{-3}
	1/500	1/70	4.375513×10^{-3}	1.910709×10^{-3}
	1/500	1/80	3.212402×10^{-3}	1.356822×10^{-3}
			$\alpha = 2.4374$	$\alpha = 2.9236$
			$C_\alpha = 138.478$	$C_\alpha = 481.5463$

Table 1: Order of convergence in space with $V(x,t) = 1 + 0.1x$

Method	Δt	Δx	L_2 Error	L_1 Error
BRKC	1/6	1/700	5.653338×10^{-3}	2.079667×10^{-3}
	1/8	1/700	3.189920×10^{-3}	1.225680×10^{-3}
	1/10	1/700	2.066911×10^{-3}	8.268313×10^{-4}
	1/12	1/700	1.460440×10^{-3}	5.999894×10^{-4}
	1/14	1/700	1.094716×10^{-3}	4.562014×10^{-4}
			$\beta = 1.9385$	$\beta = 1.7867$
			$C_\beta = 0.1808$	$C_\beta = 0.0508$
FRKC	1/6	1/700	5.920335×10^{-3}	2.503178×10^{-3}
	1/8	1/700	3.310857×10^{-3}	1.400726×10^{-3}
	1/10	1/700	2.117405×10^{-3}	8.985797×10^{-4}
	1/12	1/700	1.467171×10^{-3}	6.138583×10^{-4}
	1/14	1/700	1.075166×10^{-3}	4.520550×10^{-4}
			$\beta = 2.0123$	$\beta = 2.0222$
			$C_\beta = 0.2177$	$C_\beta = 0.0939$
BE-ELLAM	1/6	1/700	6.476122×10^{-2}	2.883357×10^{-2}
	1/8	1/700	4.817777×10^{-2}	2.151369×10^{-2}
	1/10	1/700	3.836627×10^{-2}	1.716823×10^{-2}
	1/12	1/700	3.187941×10^{-2}	1.428786×10^{-2}
	1/14	1/700	2.727120×10^{-2}	1.223664×10^{-2}
			$\beta = 1.0207$	$\beta = 1.0115$
			$C_\beta = 0.4028$	$C_\beta = 0.1764$

Table 2: Order of convergence in time with $V(x,t) = 1 + 0.1x$

Method	Δt	Δx	L_2 Error	L_1 Error
BRKC	1/500	1/60	6.117323×10^{-3}	2.475200×10^{-3}
	1/500	1/70	3.495166×10^{-3}	1.323890×10^{-3}
	1/500	1/80	2.429728×10^{-3}	9.213634×10^{-4}
	1/500	1/90	1.847878×10^{-3}	6.923624×10^{-4}
	1/500	1/100	1.408213×10^{-3}	5.172978×10^{-4}
			$\alpha = 2.8265$	$\alpha = 2.9903$
			$C_\alpha = 610.3031$	$C_\alpha = 475.0919$
FRKC	1/500	1/60	1.159784×10^{-2}	5.085293×10^{-3}
	1/500	1/70	8.458101×10^{-3}	3.559665×10^{-3}
	1/500	1/80	5.902566×10^{-3}	2.528298×10^{-3}
	1/500	1/90	3.967780×10^{-3}	1.713444×10^{-3}
	1/500	1/100	3.488353×10^{-3}	1.511827×10^{-3}
			$\alpha = 2.4833$	$\alpha = 2.4856$
			$C_\alpha = 308.5422$	$C_\alpha = 134.2145$
BE-ELLAM	1/500	1/60	6.673372×10^{-3}	2.733189×10^{-3}
	1/500	1/70	4.124203×10^{-3}	1.573640×10^{-3}
	1/500	1/80	3.124454×10^{-3}	1.199037×10^{-3}
	1/500	1/90	2.606328×10^{-3}	9.991517×10^{-4}
	1/500	1/100	2.240822×10^{-3}	8.839847×10^{-4}
			$\alpha = 2.1018$	$\alpha = 2.1665$
			$C_\alpha = 33.5250$	$C_\alpha = 17.3620$

Table 3: Order of convergence in space with $V(x,t) = 1 - 0.5x$

Method	Δt	Δx	L_2 Error	L_1 Error
BRKC	1/6	1/700	3.971642×10^{-2}	1.457259×10^{-2}
	1/8	1/700	2.157900×10^{-2}	8.290132×10^{-3}
	1/10	1/700	1.387359×10^{-2}	5.448085×10^{-3}
	1/12	1/700	9.796209×10^{-3}	3.888443×10^{-3}
	1/14	1/700	7.347346×10^{-3}	2.936484×10^{-3}
			$\beta = 1.9897$	$\beta = 1.8896$
			$C_\beta = 1.3770$	$C_\beta = 0.4261$
FRKC	1/6	1/700	3.866812×10^{-2}	1.336697×10^{-2}
	1/8	1/700	2.044585×10^{-2}	7.224535×10^{-3}
	1/10	1/700	1.276627×10^{-2}	4.564537×10^{-3}
	1/12	1/700	8.764417×10^{-3}	3.148085×10^{-3}
	1/14	1/700	6.401563×10^{-3}	2.313990×10^{-3}
			$\beta = 2.1208$	$\beta = 2.0692$
			$C_\beta = 1.7050$	$C_\beta = 0.5394$
BE-ELLAM	1/6	1/700	1.267779×10^{-1}	5.017525×10^{-2}
	1/8	1/700	9.377586×10^{-2}	3.749495×10^{-2}
	1/10	1/700	7.465792×10^{-2}	3.004816×10^{-2}
	1/12	1/700	6.210892×10^{-2}	2.512159×10^{-2}
	1/14	1/700	5.320968×10^{-2}	2.160284×10^{-2}
			$\beta = 1.0242$	$\beta = 0.9941$
			$C_\beta = 0.7916$	$C_\beta = 0.2971$

Table 4: Order of convergence in time with $V(x,t) = 1 - 0.5x$

Method	Δt	Δx	L_2 Error	L_1 Error	CPU	Fig.
BRKC	1/5	1/60	8.370973×10^{-03}	3.151613×10^{-03}	1.2	-
	1/10	1/60	2.581547×10^{-03}	9.348955×10^{-04}	2.1	I.1
FRKC	1/5	1/60	8.426960×10^{-03}	3.571262×10^{-03}	0.7	-
	1/10	1/60	2.628836×10^{-03}	1.039830×10^{-03}	1.1	I.1

Table 5: Results for BRKC & FRKC. CPU is in seconds.

Method	Δt	Δx	L_2 Error	L_1 Error	CPU	Fig.
GAL	1/69	1/60	6.315931×10^{-2}	3.769911×10^{-2}	17.9	I.2a
	1/200	1/60	1.384596×10^{-2}	6.736512×10^{-3}	51.8	I.2b
	1/300	1/60	8.437177×10^{-3}	4.054622×10^{-3}	77.6	-
	1/115	1/100	3.011717×10^{-2}	1.449988×10^{-2}	49.7	-
	1/200	1/100	1.159494×10^{-2}	5.076671×10^{-3}	86.5	-
	1/300	1/100	5.493178×10^{-3}	2.319413×10^{-3}	129.2	I.2c
QPG	1/69	1/60	5.042626×10^{-2}	2.597113×10^{-2}	17.9	I.2a
	1/200	1/60	2.384423×10^{-2}	1.121906×10^{-2}	51.9	I.2b
	1/300	1/60	2.596181×10^{-2}	1.225615×10^{-2}	77.7	-
	1/115	1/100	2.564857×10^{-2}	1.212395×10^{-2}	49.8	-
	1/200	1/100	9.187296×10^{-3}	4.064321×10^{-3}	86.5	-
	1/300	1/100	6.861496×10^{-3}	2.966565×10^{-3}	129.3	I.2c
CPG	1/69	1/60	1.502762×10^{-2}	6.299219×10^{-3}	18.0	I.2a
	1/200	1/60	4.935717×10^{-3}	2.350595×10^{-3}	51.9	I.2b
	1/300	1/60	4.589138×10^{-3}	2.242219×10^{-3}	77.8	-
	1/115	1/100	5.494951×10^{-3}	2.272993×10^{-3}	50.0	-
	1/200	1/100	1.897574×10^{-3}	7.277279×10^{-4}	86.3	-
	1/300	1/100	1.080232×10^{-3}	4.393256×10^{-4}	129.3	I.2c

Table 6: Results for GAL, QPG, & CPG. CPU time is in seconds.

C	Δt	Δx	L_2 Error	L_1 Error	CPU	Fig.
1.0	1/60	1/60	1.123311×10^{-1}	6.024287×10^{-2}	68.7	I.3a
	1/120	1/60	8.824366×10^{-2}	4.589660×10^{-2}	134.3	-
	1/180	1/60	7.944206×10^{-2}	4.087597×10^{-2}	197.9	-
	1/60	1/120	8.795492×10^{-2}	4.613883×10^{-2}	141.7	-
	1/120	1/120	5.112340×10^{-2}	2.561269×10^{-2}	269.1	I.3b
	1/180	1/120	3.812530×10^{-2}	1.867242×10^{-2}	402.1	I.3c
0.1	1/60	1/60	5.241310×10^{-2}	2.723927×10^{-2}	68.6	I.3a
	1/120	1/60	3.184598×10^{-2}	1.581704×10^{-2}	133.6	-
	1/180	1/60	2.554619×10^{-2}	1.238932×10^{-2}	198.2	-
	1/60	1/120	3.683633×10^{-2}	1.838774×10^{-2}	140.4	-
	1/120	1/120	1.514924×10^{-2}	6.961759×10^{-3}	270.4	I.3b
	1/180	1/120	9.512487×10^{-3}	4.181123×10^{-3}	402.6	I.3c
0.0001	1/60	1/60	3.279756×10^{-2}	1.715544×10^{-2}	69.1	I.3a
	1/120	1/60	1.623756×10^{-2}	8.350265×10^{-3}	140.4	-
	1/180	1/60	1.156853×10^{-2}	5.913949×10^{-3}	201.2	-
	1/60	1/120	2.310494×10^{-2}	1.108312×10^{-2}	149.7	-
	1/120	1/120	7.797575×10^{-3}	3.349920×10^{-3}	284.2	I.3b
	1/180	1/120	4.380929×10^{-3}	1.731336×10^{-3}	412.4	I.3c

Table 7: Results for SDM with C=1, 0.1, & 0.0001, CPU is in seconds.

Method	Δt	Δx	L_2 Error	L_1 Error	CPU	Fig.
CGM	1/60	1/60	4.574094×10^{-2}	2.216362×10^{-2}	13.9	I.4a
	1/120	1/60	3.136981×10^{-2}	1.399978×10^{-2}	27.7	-
	1/180	1/60	2.674044×10^{-2}	1.150175×10^{-2}	41.5	-
	1/60	1/120	2.501450×10^{-2}	1.191302×10^{-2}	28.4	-
	1/120	1/120	1.025814×10^{-2}	4.547582×10^{-3}	55.3	-
	1/180	1/120	6.763004×10^{-3}	2.919515×10^{-3}	85.1	I.4b
	1/60	1/180	1.956744×10^{-2}	9.230535×10^{-3}	41.5	-
	1/120	1/180	6.110354×10^{-3}	2.687964×10^{-3}	82.9	-
	1/180	1/180	3.381005×10^{-3}	1.457474×10^{-3}	124.3	I.4c
CGM	1/60	1/60	3.418172×10^{-2}	1.749322×10^{-2}	18.1	I.4a
	1/120	1/60	2.197196×10^{-2}	1.051318×10^{-2}	36.2	-
	1/180	1/60	1.810357×10^{-2}	8.461050×10^{-3}	54.3	-
	1/60	1/120	2.206570×10^{-2}	1.083687×10^{-2}	36.2	-
	1/120	1/120	9.206862×10^{-3}	4.198669×10^{-3}	72.3	-
	1/180	1/120	6.763004×10^{-3}	2.727802×10^{-3}	85.1	I.4b
	1/60	1/180	1.855220×10^{-2}	8.954882×10^{-3}	54.3	-
	1/120	1/180	6.062851×10^{-3}	2.722088×10^{-3}	108.5	-
	1/180	1/180	3.502214×10^{-3}	1.536899×10^{-3}	162.7	I.4c

Table 8: Results for CGM & DGM, CPU is in seconds.

Method	Δt	Δx	L_2 Error	L_1 Error	CPU	Fig.
MUSCL	1/69	1/60	5.131587×10^{-2}	1.870076×10^{-2}	0.9	I.5a
	1/115	1/100	3.019053×10^{-2}	1.019578×10^{-2}	2.6	I.5b
	1/300	1/100	2.737727×10^{-2}	1.161478×10^{-2}	6.1	-
	1/229	1/200	1.327108×10^{-2}	4.449515×10^{-3}	9.4	-
	1/300	1/200	1.203944×10^{-2}	4.042067×10^{-3}	12.4	-
	1/343	1/300	7.094933×10^{-3}	2.403457×10^{-3}	21.6	-
	1/400	1/300	6.580204×10^{-3}	2.243087×10^{-3}	24.8	-
	1/500	1/300	5.879445×10^{-3}	1.997493×10^{-3}	30.8	I.5c
	1/700	1/400	3.108750×10^{-3}	1.169307×10^{-3}	58.2	-
ENO	1/69	1/60	5.096013×10^{-2}	1.966867×10^{-2}	0.9	I.5a
	1/115	1/100	3.042145×10^{-2}	9.933304×10^{-3}	2.6	I.5b
	1/300	1/100	4.772205×10^{-2}	2.364377×10^{-2}	6.6	-
	1/229	1/200	1.667658×10^{-2}	6.502723×10^{-3}	10.1	-
	1/300	1/200	1.386139×10^{-2}	5.156693×10^{-3}	13.2	-
	1/343	1/300	1.343450×10^{-2}	5.318024×10^{-3}	22.5	-
	1/400	1/300	1.251113×10^{-2}	4.970423×10^{-3}	27.1	-
	1/500	1/300	1.094915×10^{-2}	4.439829×10^{-3}	32.7	I.5c
	1/700	1/400	1.090687×10^{-2}	4.150278×10^{-3}	61.7	-

Table 9: Results for MUSCL & ENO, CPU is in seconds.

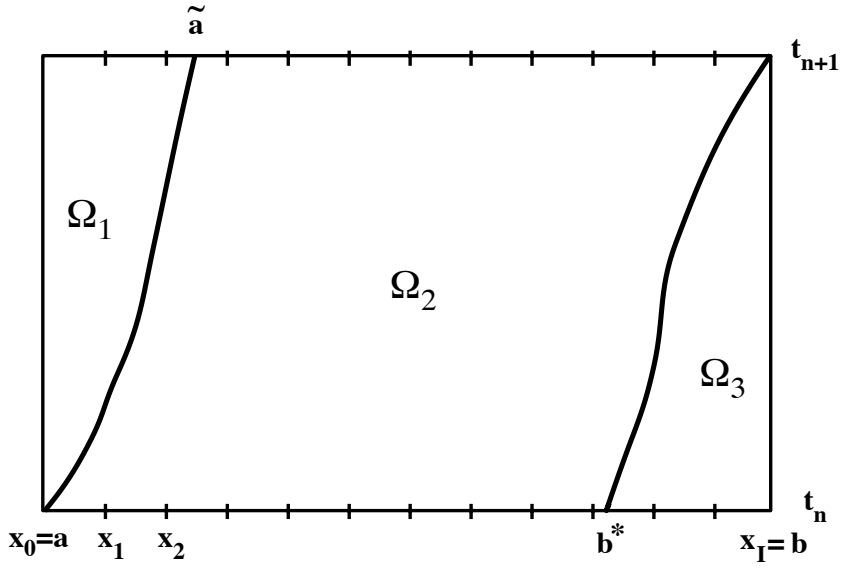

(a)

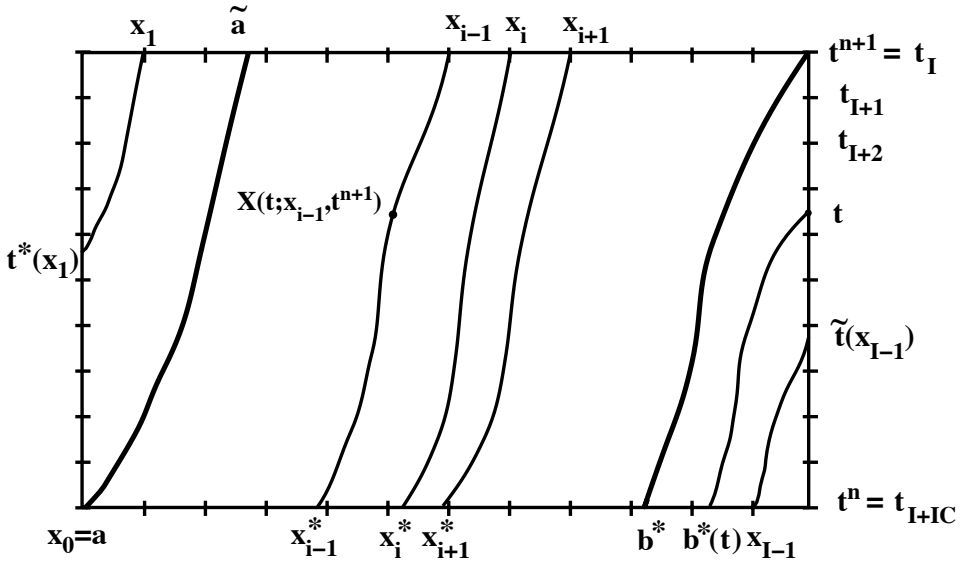

(b)

Fig 1. Partition of Ω (a) The three subdomains Ω_i $(i = 1, 2, 3)$, (b) Heads and feet of characteristics.

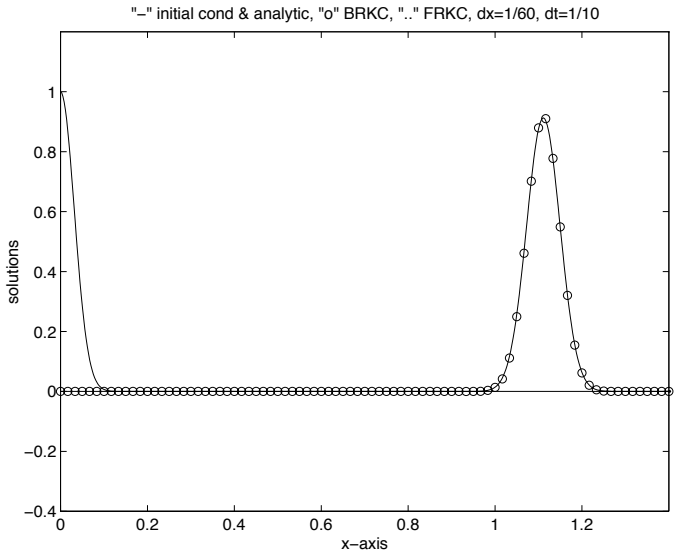

Fig I.1(a) Analytic, BRKC, & FRKC, $\Delta x = \frac{1}{60}$, $\Delta t = \frac{1}{10}$

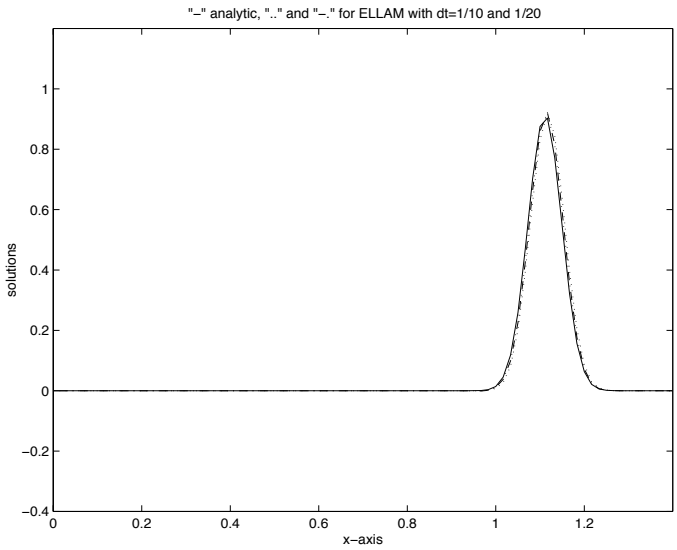

Fig I.1(b) Analytic & ELLAM, $\Delta x = \frac{1}{60}$ $\Delta t = \frac{1}{10}$ and $\frac{1}{20}$

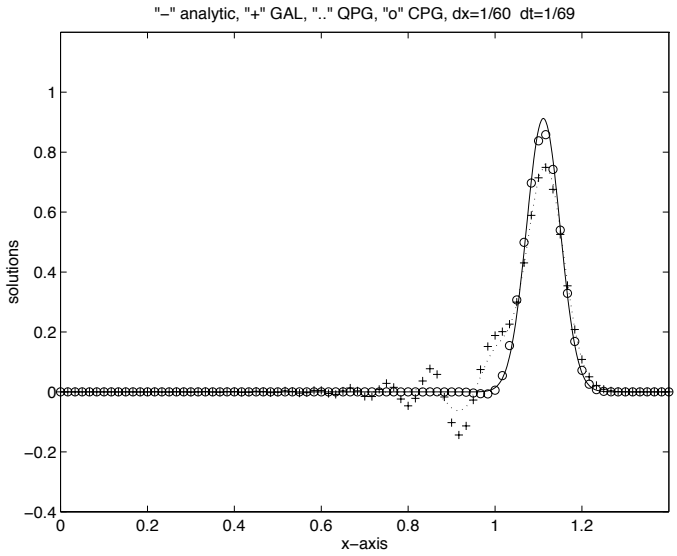

(a) $\Delta x = \frac{1}{60}$, $\Delta t = \frac{1}{69}$,

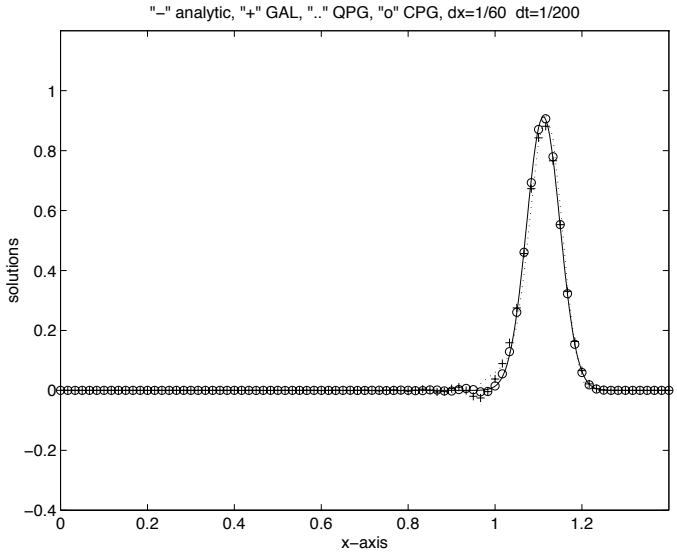

(b) $\Delta x = \frac{1}{60}$, $\Delta t = \frac{1}{200}$, and

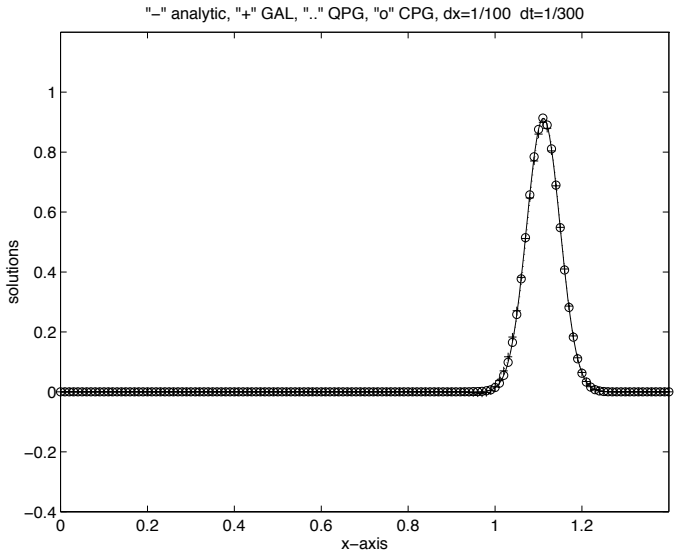

(c) $\Delta x = \frac{1}{100}$, $\Delta t = \frac{1}{300}$

Fig I.2 Galerkin, quradratic and cubic Petrov-Galerkin

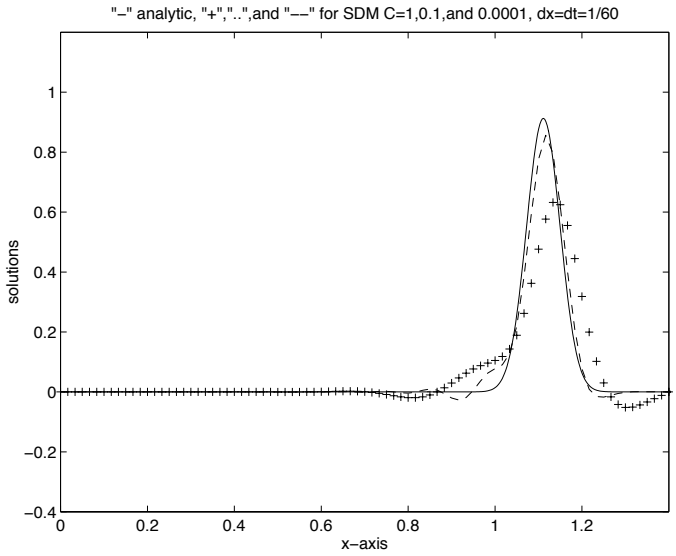

(a) $\Delta x = \Delta t = \frac{1}{60}$

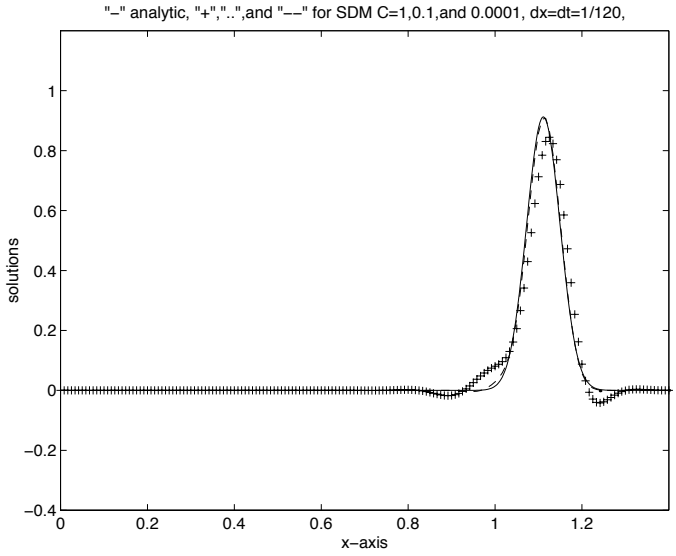

(b) $\Delta x = \Delta t = \frac{1}{120}$

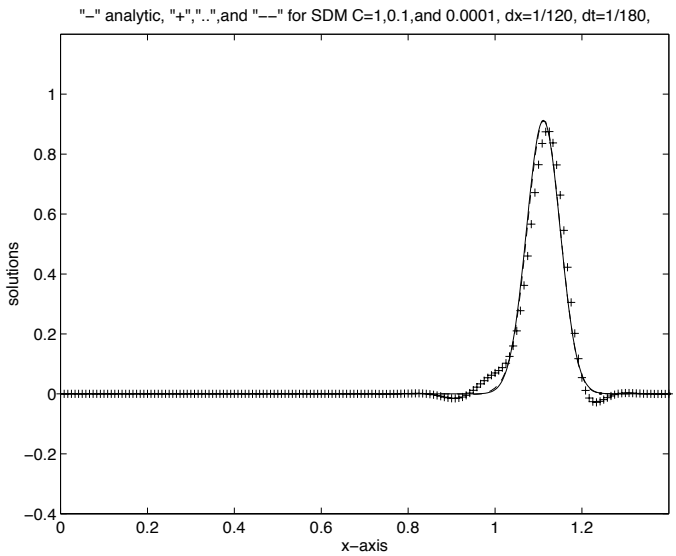

(c) $\Delta x = \frac{1}{120}$, $\Delta t = \frac{1}{180}$

Fig I.3 Streamline Diffusion Method, $C = 1$, 0.1, & 0.0001

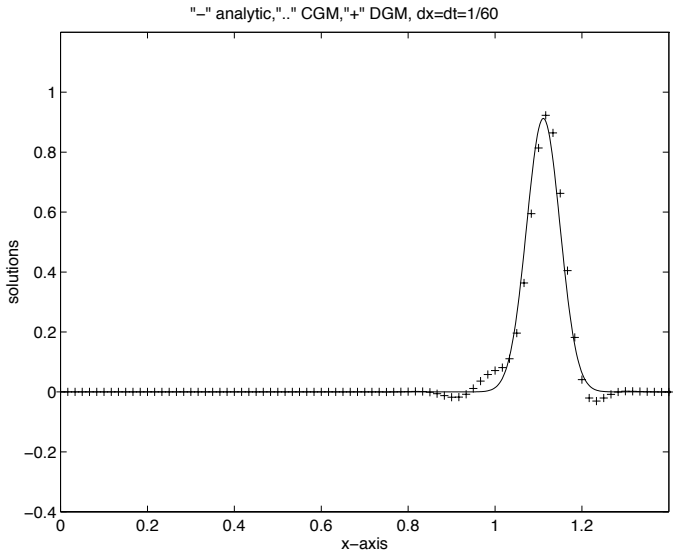

(a) $\Delta x = \Delta t = \frac{1}{60}$

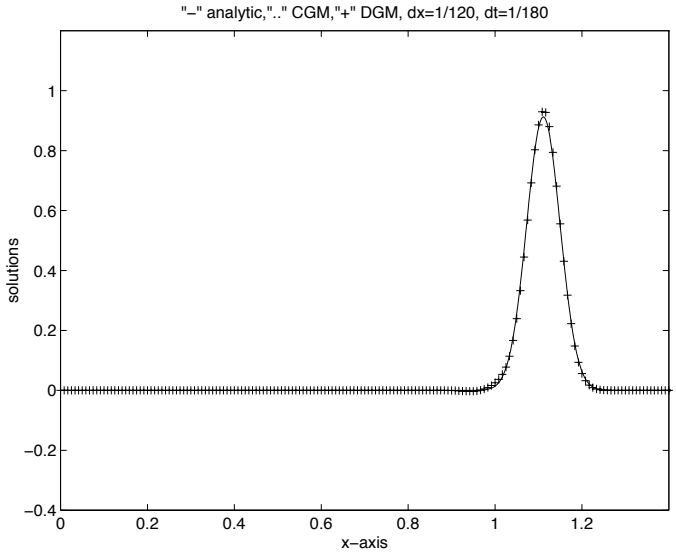

(b) $\Delta x = \frac{1}{120}$, $\Delta t = \frac{1}{180}$

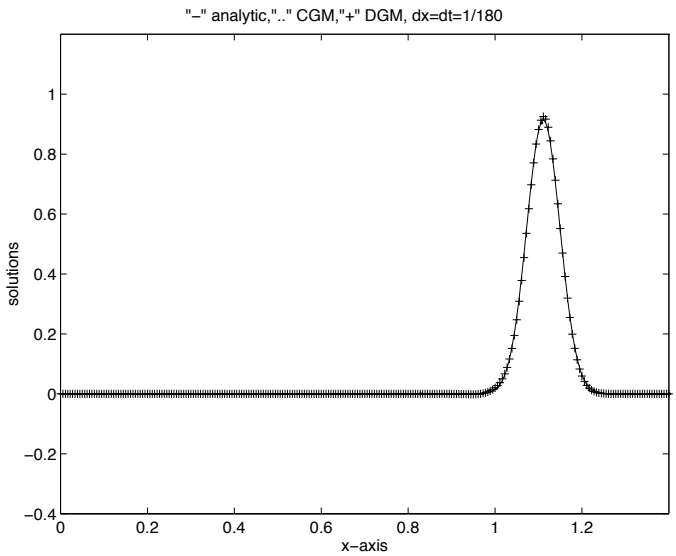

(c) $\Delta x = \Delta t = \frac{1}{180}$

Fig I.4 Continuous and discontinuous Galerkin methods

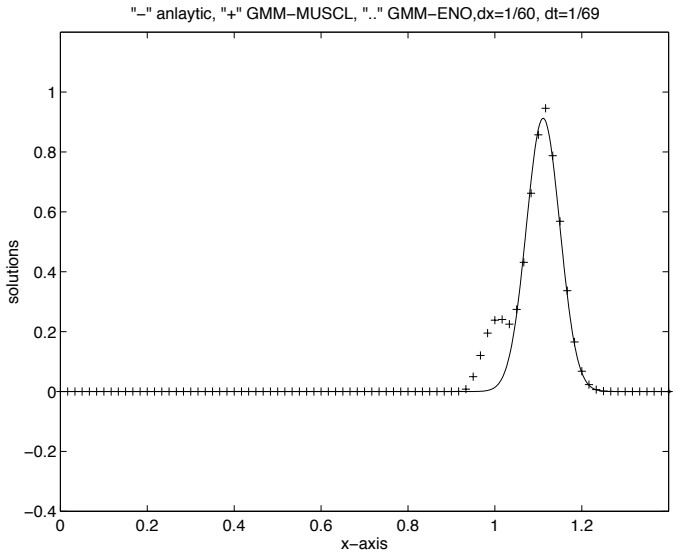

(a) $\Delta x = \frac{1}{60}$, $\Delta t = \frac{1}{69}$

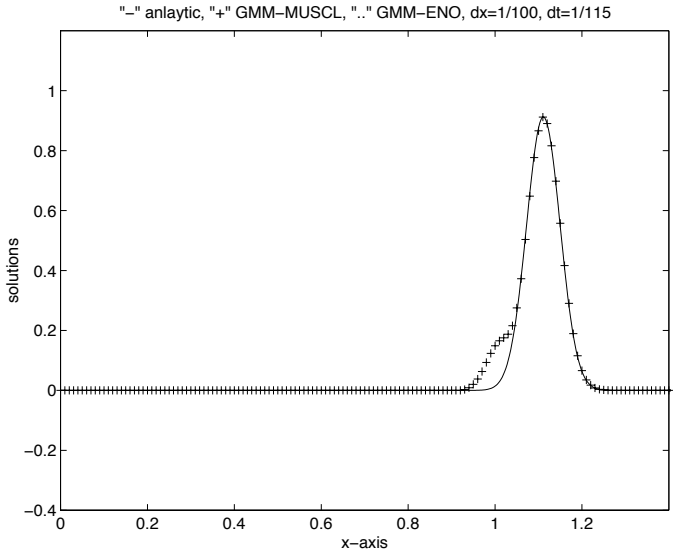

(b) $\Delta x = \frac{1}{100}$, $\Delta t = \frac{1}{115}$

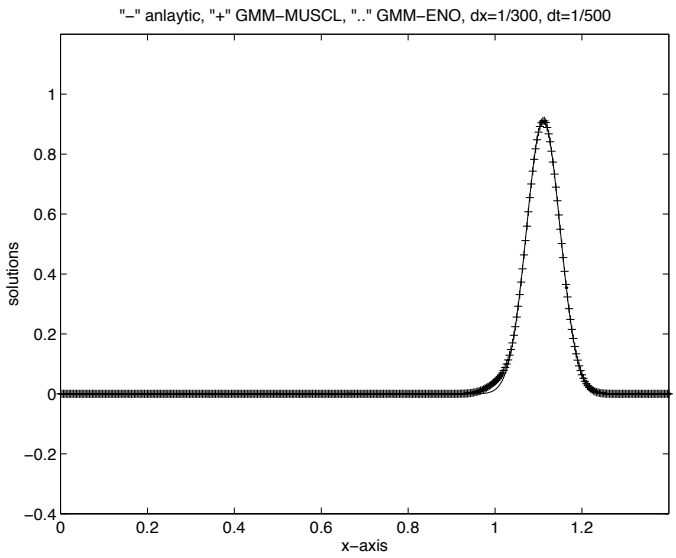

(c) $\Delta x = \frac{1}{300}$, $\Delta t = \frac{1}{500}$

Fig I.5 High resolution methods MUSCL and ENO

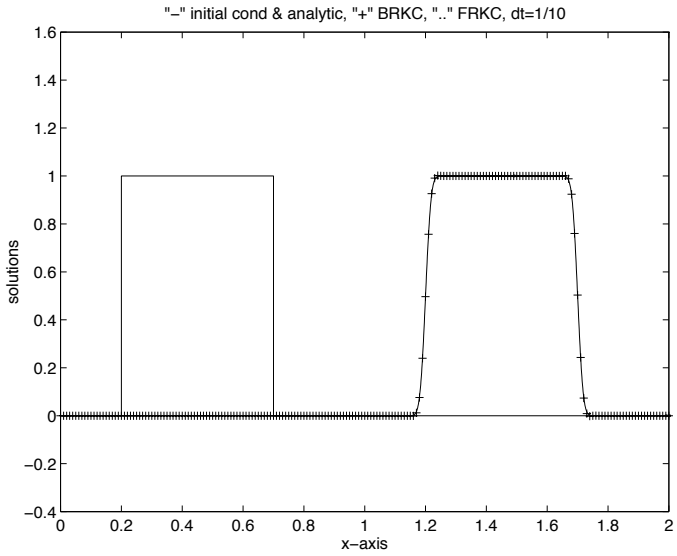

Fig II.1 BRKC, FRKC, & Anal, $\Delta x = \frac{1}{100}$, $\Delta t = \frac{1}{10}$

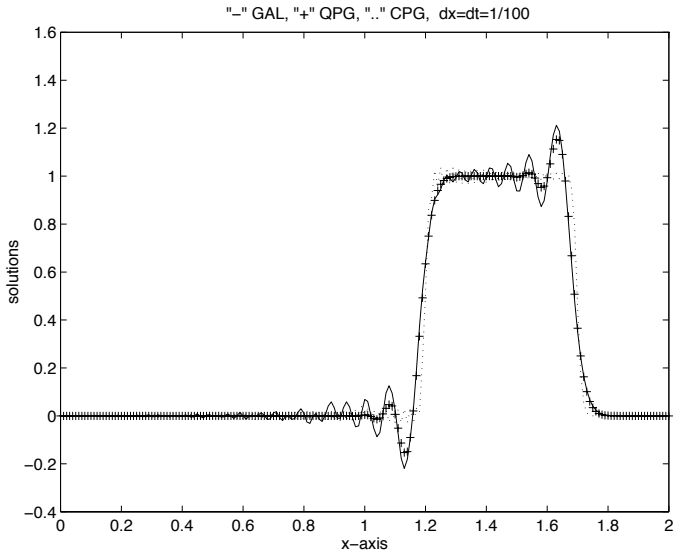

(a) $\Delta x = \Delta t = \frac{1}{100}$

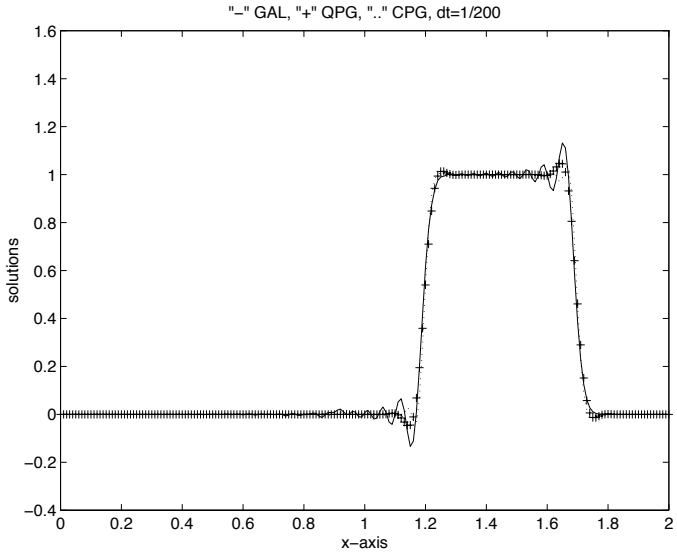

(b) $\Delta x = \frac{1}{100}$, $\Delta t = \frac{1}{200}$

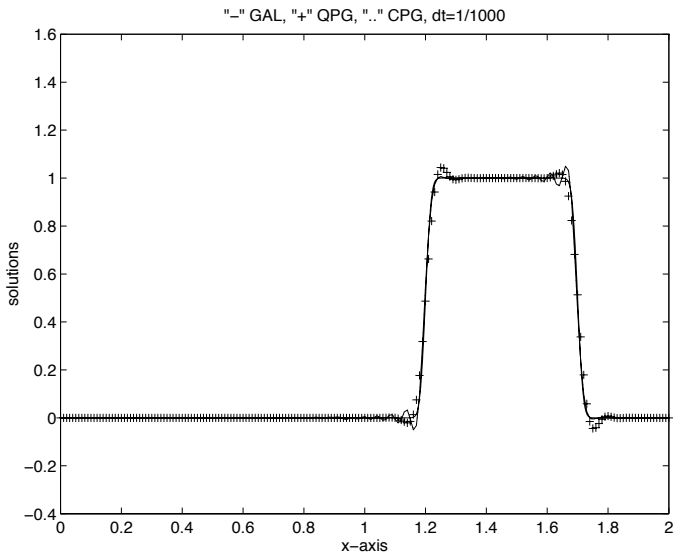

(c) $\Delta x = \frac{1}{100}$, $\Delta t = \frac{1}{1000}$

Fig II.2 Galerkin, quradratic and cubic Petrov-Galerkin

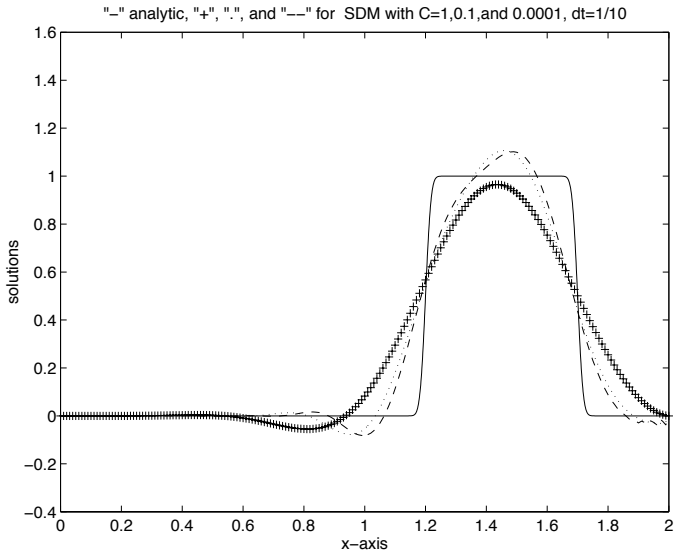

(a) $\Delta x = \frac{1}{100}$,$\Delta t = \frac{1}{10}$

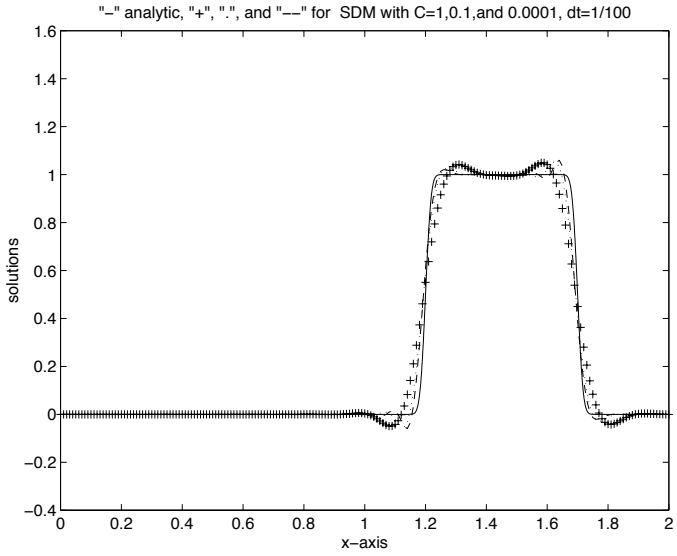

(b) $\Delta x = \Delta t = \frac{1}{100}$

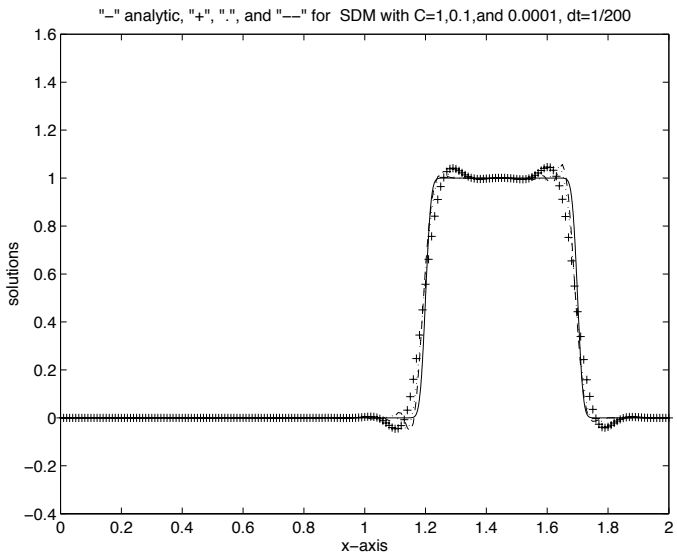

(c) $\Delta x = \frac{1}{100}$, $\Delta t = \frac{1}{200}$

Fig II.3 Streamline Diffusion Method,$C = 1$, 0.1, & 0.0001

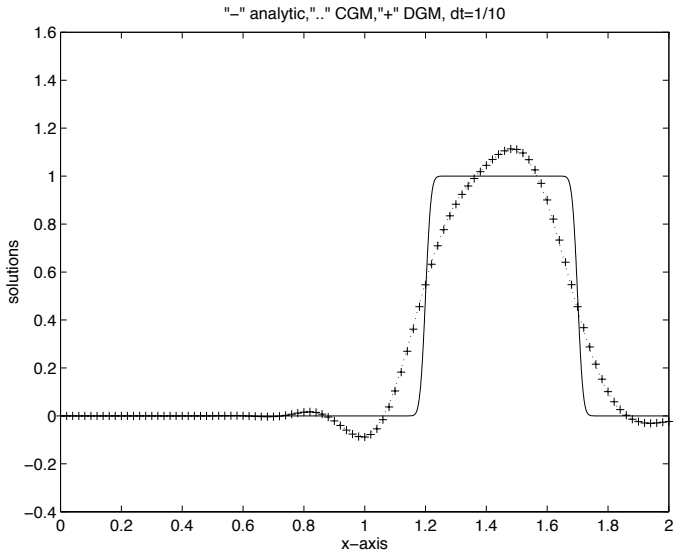

(a) $\Delta x = \frac{1}{100}$, $\Delta t = \frac{1}{10}$

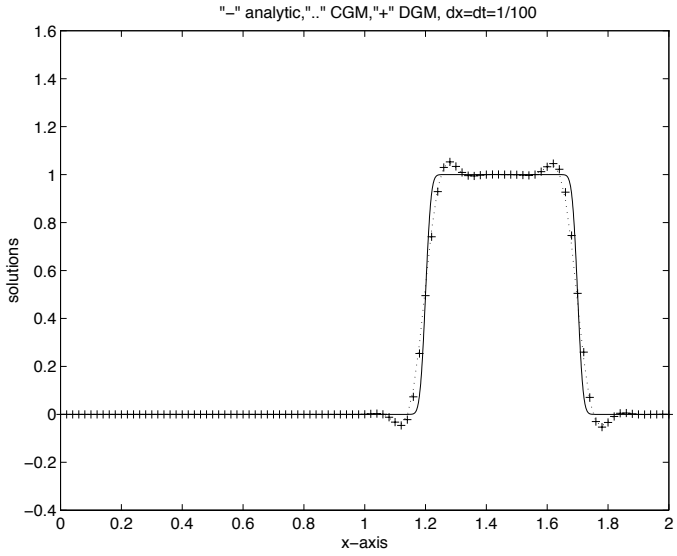

(b) $\Delta x = \Delta t = \frac{1}{100}$

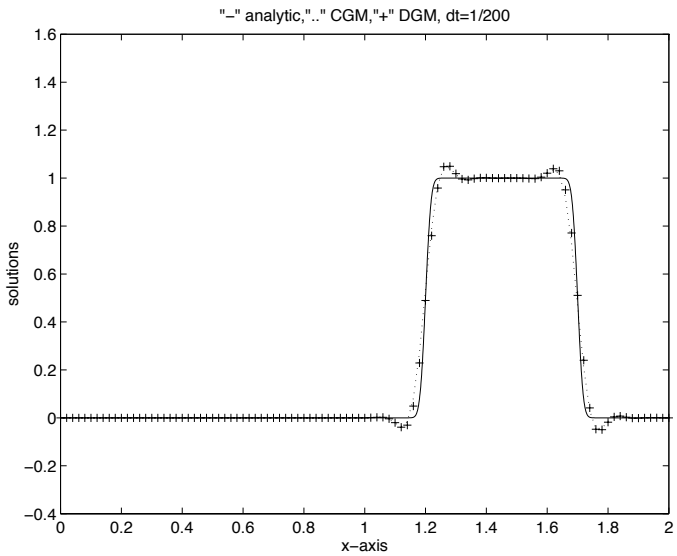

(c) $\Delta x = \frac{1}{100}$, $\Delta t = \frac{1}{200}$

Fig II.4 Continuous and discontinuous Galerkin methods

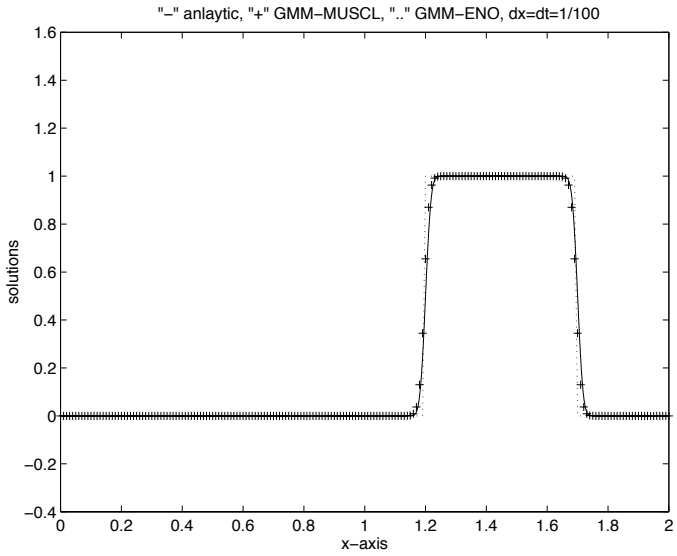

(a) $\Delta x = \Delta t = \frac{1}{100}$

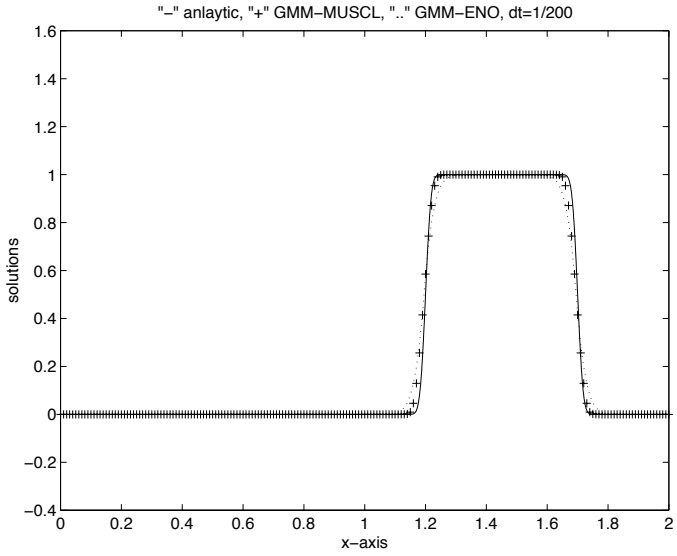

(b) $\Delta x = \frac{1}{100}$, $\Delta t = \frac{1}{200}$

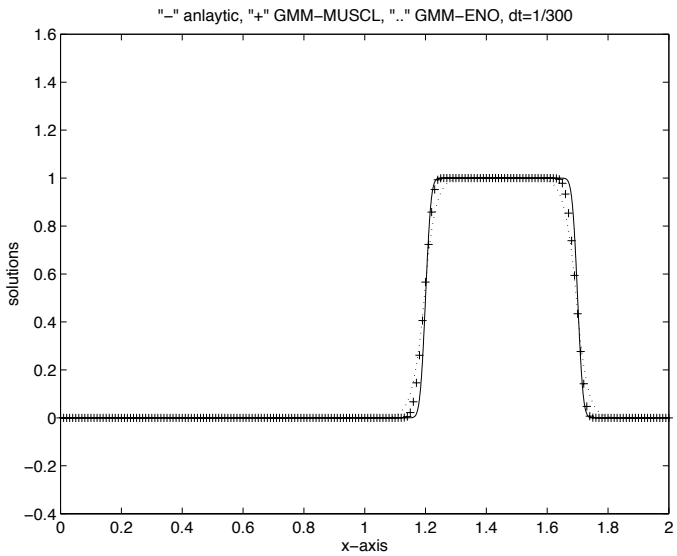

(c) $\Delta x = \frac{1}{100}$, $\Delta t = \frac{1}{300}$

Fig II.5 High resolution methods MUSCL and ENO